

Emergent Low-Rank Training Dynamics in MLPs with Smooth Activations

Alec S. Xu[†], Can Yaras, Matthew Asato, Qing Qu, Laura Balzano

University of Michigan

[†] Corresponding author

Abstract

Recent empirical evidence has demonstrated that the training dynamics of large-scale deep neural networks occur within low-dimensional subspaces. While this has inspired new research into low-rank training, compression, and adaptation, theoretical justification for these dynamics in nonlinear networks remains limited. To address this gap, this paper analyzes the learning dynamics of multi-layer perceptrons (MLPs) under gradient descent (GD). We demonstrate that the weight dynamics concentrate within invariant low-dimensional subspaces throughout training. Theoretically, we precisely characterize these invariant subspaces for two-layer networks with smooth nonlinear activations, providing insight into their emergence. Experimentally, we validate that this phenomenon extends beyond our theoretical assumptions. Leveraging these insights, we empirically show there exists a low-rank MLP parameterization that, when initialized within the appropriate subspaces, matches the classification performance of fully-parameterized counterparts on a variety of classification tasks.

Keywords: Deep Learning, Gradient Descent, Low-Dimensional Subspaces

Date: February 9, 2026

Correspondence: alecx@umich.edu

Resources: Code to be released

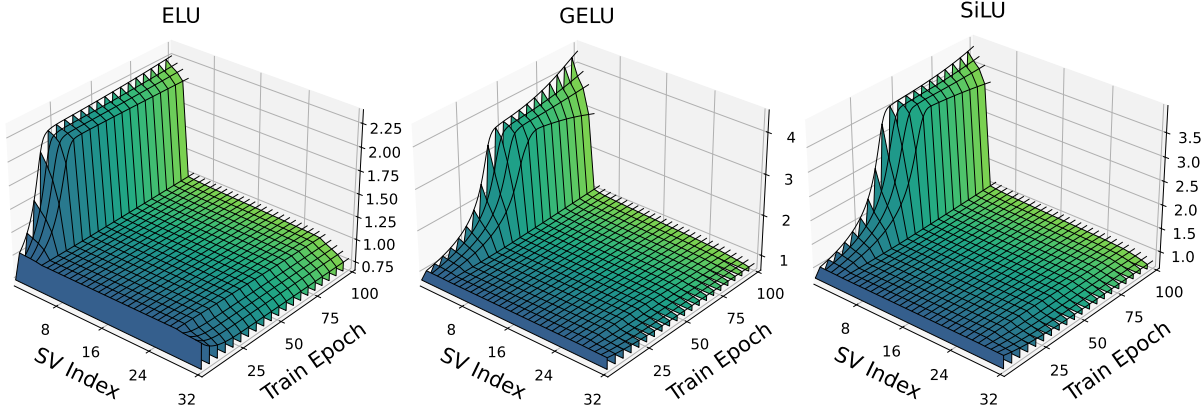


Figure 1: **Low rank updates in MLPs with smooth activation functions.** Each plot shows how the singular values of the first layer (out of four layers total) evolve throughout training in MLPs with ELU, GELU, and SiLU activation functions, which are all smooth. We trained each MLP on synthetic data and squared-error loss using gradient descent. Specific experimental details and additional plots of the deeper layer singular values are in Appendix A.1.

Contents

1	Introduction	3
2	Problem Setup	3
2.1	Case Study: Smooth Activations Encourage Lower-Rank Training Dynamics	4
3	Analysis on Two-Layer Nonlinear Networks	5
3.1	Definitions and Assumptions	5
3.2	Main Results	6
3.3	Proof Sketch of Theorem 3.5	8
4	Empirical Observations Beyond Theory	8
4.1	Deeper Networks	9
4.2	Loss Function, Optimizer, and Unwhitened Data	10
5	Low-Rank Parameterization in MLPs	10
5.1	Experiments	11
5.1.1	Fashion MNIST using MLPs	11
5.1.2	CIFAR-10 using VGG-16	12
6	Related Work	13
6.1	Low-Dimensional Learning in Neural Networks	13
6.2	Low Rank Gradients in Neural Networks	13
6.3	Implicit Bias in Two-Layer Networks	14
7	Conclusion	14
A	Additional Simulation Details and Results	18
A.1	Additional Details and Results for Figure 2	18
A.2	Experimental Details for Figure 3	21
A.3	Experimental Details for Section 4	21
B	Why Activation Smoothness Matters: Some Intuition	21
B.1	Verifying Proposition B.1	22
C	Empirical Justifications for Assumption 3.4	23
D	Proofs for Theorem 3.5	23
D.1	Notation and Assumptions	24
D.2	Analytical Gradient Form	25
D.3	Supporting Results	25
D.3.1	Auxiliary Results	25
D.3.2	Gradient Bounds	28
D.3.3	Gradient Singular Values and Subspaces	29
D.4	Proof of Theorem 3.5	32
E	Proof of Proposition B.1	36
F	Low-Rank MLP Ablations	39
F.1	Subspace Initialization	40
F.2	Width Ablation	40

1 Introduction

Recently, low-rank approaches have achieved great success in training and fine-tuning large neural networks. For example, low-rank adaptation (LoRA) (Hu et al., 2022) has recently emerged as a popular fine-tuning technique for large language models (LLMs) by adding a low-rank adapter to frozen pre-trained weights. Other works have proposed projecting the parameters (Li et al., 2022; Zhang et al., 2023) or the optimizer states (Zhao et al., 2024; Robert et al., 2025; Zhu et al., 2025; Rajabi et al., 2025) onto low-dimensional subspaces, and then updating the parameters or optimizer states there — see Balzano et al. (2025) for a survey.

Empirical observations indicate large model training and fine-tuning naturally occur within low dimensional subspaces (Gur-Ari et al., 2018; Li et al., 2018; Larsen et al., 2022), which potentially explains the success of the aforementioned low-rank training approaches. However, a precise characterization of *which* subspaces the optimization occurs within remains unclear. To address this question, Yaras et al. (2023, 2024); Kwon et al. (2024) proved that when deep *linear* networks are trained via gradient descent (GD), the weights are updated within fixed subspaces that depend on the weights at initialization. However, practical neural networks are highly nonlinear, and no work has investigated how introducing nonlinearities in the network impacts this phenomenon. To this end, we extend these works by focusing on multi-layer perceptrons (MLPs). We find that when the MLP output dimension is much smaller than the input and hidden dimensions, and the activation function is smooth, the training dynamics are highly concentrated within unchanging low-dimensional subspaces. Our contributions are as follows:

Contributions

- **Theoretical analysis on two-layer networks (Section 3).** We provide the first theoretical analysis on this phenomenon on two-layer networks trained via GD. Specifically, we show there exists a fixed subspace such that, in each GD step, the change of the first-layer weights in this subspace is bounded. This subspace depends on the first layer’s weights and gradient at initialization.
- **Low-rank training beyond theory (Section 4).** We conduct simulations demonstrating low-rank training dynamics also emerge beyond our theoretical setting. Particularly, we demonstrate empirically that the GD updates of the deeper layers *also* occur within low-dimensional subspaces that again depend on the network initialization. We also show this phenomenon approximately holds for networks trained using SGD with momentum and Adam.
- **Low-rank MLP parameterizations (Section 5).** Based on the previous insights, we empirically show there exists a low-rank MLP parameterization that, if initialized in the appropriate subspaces, achieves near-equivalent performance compared to their fully parameterized counterparts under the same training setting. We conduct experiments on Fashion MNIST and CIFAR-10 using deep MLPs demonstrating this near-equivalence and the importance of the initialization.

Related work. There have been several recent works on low-dimensional learning in deep networks (Li et al., 2018, 2022; Larsen et al., 2022; Schottöfer et al., 2022; Yaras et al., 2024; Kwon et al., 2024), as well as low-rank gradients in nonlinear networks (Ba et al., 2022; Zhao et al., 2024; Jaiswal et al., 2025; Sonthalia et al., 2025). Another relevant line of work is the implicit bias towards low-rank weights in nonlinear networks (Frei et al., 2023; Kou et al., 2023; Timor et al., 2023; Min et al., 2024). See Section 6 for more detailed discussions on these related works.

2 Problem Setup

Here, we set up and motivate our problem of interest.

Notation. We use unbolted letters x, X for scalars, bold lower case letters \mathbf{x} for vectors, and bold capital letters \mathbf{X} for matrices. For some $N \in \mathbb{N}$, $[N]$ denotes the set $\{1, 2, \dots, N\}$. For scalars a, b , we say $a \lesssim O(b)$ if there exists a constant C s.t. $a \leq C \cdot b$, $a \gtrsim \Omega(b)$ if $a \geq C \cdot b$, and $a = \Theta(b)$ if $a = C \cdot b$. We use $\sigma_i(\mathbf{X})$, $\|\mathbf{X}\|_F$, $\|\mathbf{X}\|_1$, and $\|\mathbf{X}\|_{\max}$ to respectively denote the i^{th} singular value, Frobenius norm, matrix-1 norm, and maximum

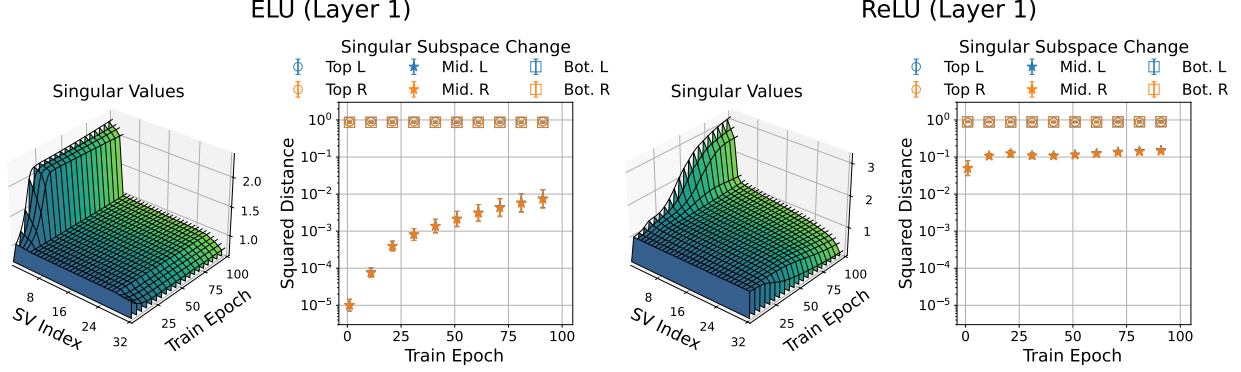


Figure 2: The middle singular subspace of the first-layer weight matrix in the ELU network evolves noticeably slower than that in the ReLU network, and the corresponding singular values remain closer to their initialization.

magnitude element. Finally, $\mathcal{R}(X)$ denotes the range (or column space) of X , and $\mathcal{R}^\perp(X)$ its orthogonal complement.

Data. We consider data with inputs $X \in \mathbb{R}^{d \times N}$ and labels $Y \in \mathbb{R}^{K \times N}$, where d is the data dimension, N is the number of data points, and K is the label dimension. We consider the case where K is much smaller compared to d and N (formally defined in Assumption 3.2). Finally, we define $p := d - 2K$.

Network architecture. We define an L -layer neural network $f_\Theta : \mathbb{R}^{d \times N} \rightarrow \mathbb{R}^{K \times N}$ as follows:

$$f_\Theta(X) = W_L \phi(W_{L-1} \phi(\dots \phi(W_1 X) \dots)), \quad (1)$$

where $\phi(\cdot)$ is the element-wise nonlinear activation function, W_l denotes the l^{th} layer's weight matrix, and $\Theta = \{W_1, \dots, W_L\}$ denote the model parameters. Here, $W_1 \in \mathbb{R}^{m_1 \times d}$, $W_l \in \mathbb{R}^{m_l \times m_{l-1}}$ for $l \in \{2, \dots, L-1\}$, and $W_L \in \mathbb{R}^{K \times m_{L-1}}$. For simplicity, we assume $m_1 = m_2 = \dots = m_{L-1} := m$.

Training. We train f_Θ defined in (1) via

$$\min_{\Theta} \mathcal{L}(\Theta) := \ell(f_\Theta(X), Y), \quad (2)$$

where \mathcal{L} is some loss function. We solve (2) through gradient descent (GD) with step size η :

$$\Theta(t+1) = \Theta(t) - \eta \nabla \mathcal{L}(\Theta(t)) \quad (3)$$

where t denotes the iteration index.

2.1 Case Study: Smooth Activations Encourage Lower-Rank Training Dynamics

To motivate our problem of interest, we present a case study showcasing when low-rank training dynamics emerge in MLPs. We trained six different MLPs using full-batch GD on synthetic classification data with $d = 32$ dimensions and $K = 4$ classes. Each MLP contained a different activation function: three had smooth activations (ELU, GELU, and SiLU), while the other three had nonsmooth ones (ReLU, Leaky-ReLU, and Randomized-ReLU, or RReLU). During training, we tracked each of the first three layers' singular values, as well as the changes in their top- K , bottom- K , and middle $d - 2K$ singular subspaces. We show results for the first layer of the ELU and ReLU networks in Figure 2, while deferring other results and experimental details to Appendix A.1.

In the ELU network's first layer, the middle $d - 2K$ singular subspace evolves very slowly throughout training, especially compared to that of the ReLU network. These singular subspace changes are also reflected

in their corresponding singular values. This is not unique to ELU and ReLU: the changes in singular values and subspaces are noticeably smaller in MLPs with smooth activations compared to nonsmooth (see Figures 8 to 10 in Appendix A.1). Thus, for MLPs with smooth activations, the training dynamics appear much more concentrated within a lower-dimensional subspace, implying **low-rank training dynamics emerge more prominently for MLPs with smooth activation functions**. Therefore, for the remainder of our study, we focus on characterizing these dynamics with such activations.

3 Analysis on Two-Layer Nonlinear Networks

In this section, we provide our main theoretical result characterizing low-rank training dynamics in two-layer networks.

3.1 Definitions and Assumptions

In this section, we provide some preliminary definitions, and then state and discuss our assumptions. We first define quantities that measure the alignment between two subspaces.

Definition 3.1 (Principal angles between subspaces). Let $\mathbf{U}_1, \mathbf{U}_2 \in \mathbb{R}^{d \times r}$ be orthonormal bases of two r -dimensional subspaces of \mathbb{R}^d . Then, for all $i \in [r]$, the i^{th} principal angle θ_i between \mathbf{U}_1 and \mathbf{U}_2 is defined as such:

$$\theta_i = \arccos(\sigma_i(\mathbf{U}_1^\top \mathbf{U}_2)) \in [0, \pi/2].$$

We also measure the alignment between \mathbf{U}_1 and \mathbf{U}_2 through the following metric:

$$\|\sin \Theta(\mathbf{U}_1, \mathbf{U}_2)\|_2 := \sqrt{\sum_{i=1}^r \sin^2(\theta_i)} \in [0, \sqrt{r}].$$

Smaller principal angles θ_i indicate \mathbf{U}_1 and \mathbf{U}_2 are well aligned, and also leads to smaller $\|\sin \Theta(\mathbf{U}_1, \mathbf{U}_2)\|_2$. Thus, smaller $\|\sin \Theta(\mathbf{U}_1, \mathbf{U}_2)\|_2$ indicates greater alignment between \mathbf{U}_1 and \mathbf{U}_2 .

We now provide our assumptions. First, we state our assumptions on the input data \mathbf{X} and labels \mathbf{Y} .

Assumption 3.2 (Input data). The data $\mathbf{X} \in \mathbb{R}^{d \times N}$ is whitened, and the label dimension K satisfies $K < d/2$.

Before proceeding, we briefly discuss Assumption 3.2.

• **Whitened input data.** Several previous works on neural network analyses assume whitened input data, e.g., Arora et al. (2019); Braun et al. (2022); Yaras et al. (2023); Dominé et al. (2025). In Section 4.2, we empirically observe this phenomenon approximately holds for unwhitened \mathbf{X} .

• **Small output dimension $K \ll d$.** We consider a setting where the $K \ll d$, which is commonly studied. For instance, Andriopoulos et al. (2024) studied neural collapse (Papyan et al., 2020) in this exact setting. Classification is another example of where this setting is common, as K represents the number of classes. In our analysis, we show K governs the rank of the low-rank training dynamics.

Next, we state our assumptions on the network architecture and training.

Assumption 3.3 (Network architecture and training). The network (1) contains $L = 2$ layers, i.e., $f_{\Theta}(\mathbf{X}) =: f_{W_1}(\mathbf{X}) = W_2 \phi(W_1 \mathbf{X})$, with $W_1 \in \mathbb{R}^{m \times d}$ and $W_2 \in \mathbb{R}^{K \times m}$. Furthermore,

- The width m satisfies $m \geq d$,
- The activation function ϕ satisfies $\phi(0) = 0$, $|\phi'(x)| \leq \beta$, and $|\phi''(x)| \leq \mu$ for all $x \in \mathbb{R}$.
- The network is trained using GD with step size η on the squared error loss:

$$\min_{W_1} \mathcal{L}(W_1) = \frac{1}{2} \|f_{W_1}(\mathbf{X}) - \mathbf{Y}\|_F^2, \quad (4)$$

where W_2 is fixed during training and is full row rank.

We provide some brief remarks on Assumption 3.3.

- **Squared-error loss.** Several works on neural network analyses considered squared-error loss (Oymak and Soltanolkotabi, 2019, 2020; Bao et al., 2023; Chistikov et al., 2023), even for classification tasks (Hui and Belkin, 2021; Zhou et al., 2022; Wang et al., 2023). In Section 4.2, we empirically observe in classification tasks, training on cross-entropy loss leads to a similar low-rank training phenomenon.
- **Fixed second layer.** In our problem, we aim to show the weight matrices in nonlinear networks mostly get updated in low-dimensional subspaces. Since W_2 is of size $K \times m$, where $K \ll d \leq m$, we focus our analysis on the GD dynamics of W_1 , which is of size $m \times d$. To simplify the analysis, we keep W_2 fixed during training. A fixed second layer is a standard assumption in two-layer network analyses, e.g., Frei et al. (2023); Kou et al. (2023); Boursier et al. (2022); Oymak and Soltanolkotabi (2019, 2020); Gopalani and Mukherjee (2025).

Finally, we introduce the following technical assumptions, which we empirically support in Appendix C.

Assumption 3.4. Define $\Delta_2(t) = W_2\phi(W_1(t)X) - Y$ and $G_1(t) = \nabla_{W_1}\mathcal{L}(W_1(t))$. For all $t \geq 0$,

- $\|\Delta_2(t)\|_{\max} \leq M$ for some finite constant M , and
- there exist constants G_1, G_2 , and G_3 such that $G_1(t)$ satisfies the following:

$$\begin{aligned} \frac{\|G_1(t)\|_F}{\|G_1(0)\|_F} &\leq G_1 \cdot (1 - \Theta(\eta))^{\Theta(t)}, \\ \frac{\sigma_i(G_1(t))}{\sigma_i(G_1(0))} &\leq G_2 \cdot \frac{\|G_1(t)\|_F}{\|G_1(0)\|_F}, \quad \text{for all } i \leq K, \text{ and} \\ \sigma_K(W_2^\top YX^\top) - \sigma_{K+1}(G_1(t)) &\geq G_3 \cdot \sigma_K(W_2^\top YX^\top) \end{aligned}$$

We briefly discuss Assumption 3.4 below, and provide empirical justification for the second part in Appendix C.

- **Bounded residual elements throughout training.** This assumption states the maximum magnitude element in the residual is bounded by some finite constant, which we make for technical convenience. This assumption is quite mild, since if we did have $\|\Delta_2(t)\|_{\max} \rightarrow \infty$, then we would also have $\frac{1}{2}\|\Delta_2(t)\|_F^2 = \mathcal{L}(W_1(t)) \rightarrow \infty$.
- **Gradient norm and singular values.** This assumption initially appears quite strict since our objective is nonconvex. However, in our specific setting, we empirically observe that as GD converges to a stationary point, the gradient norm and singular values decay at similar rates; see Figure 12 in Appendix C. We also assume the tail singular values of $G_1(t)$ are much smaller than $\sigma_K(W_2^\top YX^\top)$ to make the analysis tractable. In particular, it allows us to use Wedin's Sin Theorem (Wedin, 1972) to upper bound the change in singular subspace alignment. Figure 13 shows this assumption holds in our setting.

3.2 Main Results

In this section, we present our main theoretical result.

Theorem 3.5 (Simplified). Recall $p := d - 2K$, where d is the data dimension, and K is the label dimension. Let $L_{1,1}(t)$ and $R_{1,1}(t)$ denote top- K left and right singular subspaces of $\nabla_{W_1}\mathcal{L}(W_1(t))$, and define the singular subspace alignment to initialization at iteration t as

$$A(t) := \max \left\{ \|\sin \Theta(L_{1,1}(t), L_{1,1}(0))\|_2, \|\sin \Theta(R_{1,1}(t), R_{1,1}(0))\|_2 \right\}.$$

Suppose $W_1(0)$ satisfies $W_1^\top(0)W_1(0) = \epsilon^2 I_d$ with $\epsilon \lesssim O(\sigma_K(W_2^\top YX^\top))$, and let the step size satisfy $\eta \lesssim \min \left\{ 1, \frac{1}{\Omega(\|W_2\|_1 + \sigma_1^2(W_2))} \right\}$. Then, there exist orthogonal matrices $U \in \mathbb{R}^{m \times m}$ and $V \in \mathbb{R}^{d \times d}$ that only depend on

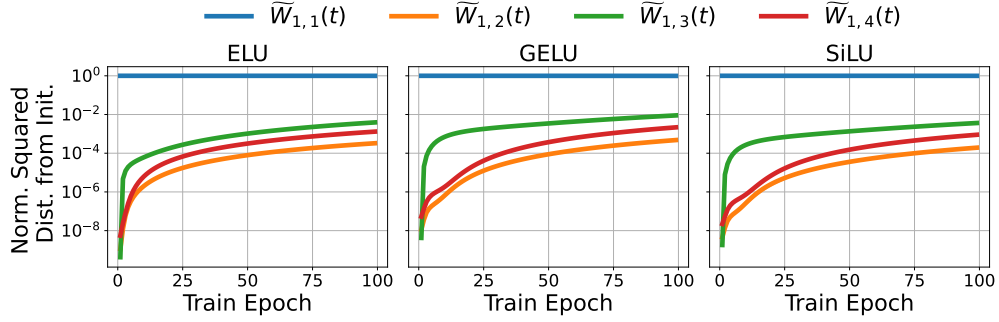


Figure 3: Under our exact theoretical setting, $\widetilde{W}_{1,1}(t)$ accounts for almost all of the change in $\widetilde{W}_1(t)$, and thus $W_1(t)$.

$W_1(0)$ and $G_1(0)$ such that, for all $t \geq 0$, $W_1(t)$ admits the following decomposition:

$$W_1(t) = U \widetilde{W}_1(t) V^\top = U \begin{bmatrix} \widetilde{W}_{1,1}(t) & \widetilde{W}_{1,2}(t) \\ \widetilde{W}_{1,3}(t) & \widetilde{W}_{1,4}(t) \end{bmatrix} V^\top,$$

where $\widetilde{W}_{1,1}(t) \in \mathbb{R}^{(m-p) \times 2K}$, $\widetilde{W}_{1,2}(t) \in \mathbb{R}^{(m-p) \times p}$, $\widetilde{W}_{1,3}(t) \in \mathbb{R}^{p \times 2K}$, and $\widetilde{W}_{1,4}(t) \in \mathbb{R}^{p \times p}$, with

$$\widetilde{W}_{1,2}(0) = \mathbf{0}, \quad \widetilde{W}_{1,3}(0) = \mathbf{0}, \quad \frac{\|\widetilde{W}_{1,4}(0)\|_F}{\sqrt{p}} = \epsilon,$$

and

$$\frac{\|\widetilde{W}_{1,i}(t+1) - \widetilde{W}_{1,i}(t)\|_F}{\sqrt{p}} \lesssim \eta \cdot \rho(t),$$

for all $i \in \{2, 3, 4\}$, where

$$\rho(t) = \sqrt{\sigma_1^2(G_1(t)) \cdot \frac{A^2(t)}{p} + \sigma_{K+1}^2(G_1(t))} \leq \begin{cases} C_1 \epsilon & t = 0 \\ C_2 \cdot (1 - \Theta(\eta))^{\Theta(t)} \cdot \left(1 - (1 - \Theta(\eta))^{\Theta(t)}\right) & t \geq 1 \end{cases}$$

for some constants C_1, C_2 .

Discussion on Theorem 3.5. We briefly discuss the implications of our main theoretical result — for ease of exposition, we focus on the case where $m = d$. Let $U := [U_1 \ U_2]$ and $V = [V_1 \ V_2]$, where $U_1 \in \mathbb{R}^{d \times 2K}$, $U_2 \in \mathbb{R}^{d \times p}$, $V_1 \in \mathbb{R}^{d \times 2K}$, and $V_2 \in \mathbb{R}^{d \times p}$ all have orthonormal columns, where again $p = d - 2K$. From Theorem 3.5, we have

$$W_1(t) = \underbrace{U_1 \widetilde{W}_{1,1}(t) V_1^\top}_{\text{rank } 2K} + U_1 \widetilde{W}_{1,2}(t) V_2^\top + U_2 \widetilde{W}_{1,3}(t) V_1^\top + U_2 \widetilde{W}_{1,4}(t) V_2^\top.$$

For $i \neq 1$, we refer to $\widetilde{W}_{1,i}(t)$ as the **perturbation terms**.

- **Low rank training via gradient subspace alignment and low rank gradients.** Theorem 3.5 shows that the alignment between the gradient singular subspaces at iteration t vs. initialization determines how large the perturbation terms get updated. In the early training stages, the singular subspaces are well-aligned with the corresponding singular subspaces at initialization. As training progresses, these singular subspaces become less aligned, as reflected in the $1 - \lambda(\eta)^{\Theta(t)}$ term. However, the top- K gradient singular values simultaneously decay as GD converges to a stationary point, as reflected in the $\lambda(\eta)^{\Theta(t)}$ term. Small changes in the perturbation terms also rely on the gradient being approximately rank- K . If $\sigma_{K+1}(G_1(t))$ is “large,” then the perturbation terms could change more significantly at that iteration.

- **Role of initialization scale.** Frei et al. (2023); Kou et al. (2023) empirically observed GD converges to lower stable rank solutions at smaller initialization scales. Theorem 3.5 offers theoretical insight into why this is the case. At initialization, we have $\|\widetilde{W}_{1,4}(0)\|_F/\sqrt{p} = \epsilon$, and after the first GD step, the norms of the perturbation terms grow by at most $\mathcal{O}(\epsilon)$, which is reflected in the $C_1\epsilon$ term. For larger ϵ , the perturbation terms potentially undergo larger growth after a single step, thus potentially increasing the stable rank of $W_1(t)$.

Experimental verification. We trained the first layer of two layer networks of various activations under the exact setting of Theorem 3.5; we defer specific experimental details to Appendix A.2. Figure 3 shows the squared distance of each $\widetilde{W}_{1,i}(t)$ from $\widetilde{W}_{1,i}(0)$ normalized by the squared distance between $\widetilde{W}_1(t)$ and $\widetilde{W}_1(0)$, i.e., $\|\widetilde{W}_{1,i}(t) - \widetilde{W}_{1,i}(0)\|_F^2/\|\widetilde{W}_1(t) - \widetilde{W}_1(0)\|_F^2$, averaged over 10 trials. Clearly, for all activations, $\widetilde{W}_{1,1}(t)$ accounts for almost all of the change in $\widetilde{W}_1(t)$, and thus $W_1(t)$. These results support the main message in Theorem 3.5: **each GD update mostly occurs in a low-dimensional subspace.**

3.3 Proof Sketch of Theorem 3.5

Here, we summarize the proof strategy for Theorem 3.5, and defer the full proof to Appendix D.

Approximate low-rank gradient at initialization. First, we show $G_1(0)$ is approximately rank- K at small initialization scale ϵ . Recall $W_1(0) = \epsilon Q \in \mathbb{R}^{m \times d}$ for some Q with orthonormal columns. Defining $\Delta_2(0) = W_2\phi(W_1(0)X) - Y$, we have,

$$G_1(0) = (W_2^\top \Delta_2(0) \odot \phi'(W_1(0)X)) X^\top.$$

Next, we have that $\phi'(W_1(0)X) = \phi'(\epsilon QX)$ lies within an $\Theta(\epsilon)$ interval of $\phi'(0) \cdot \mathbf{1}_m \mathbf{1}_N^\top$, and so $\phi'(W_1(0)X) \approx \phi'(0) \cdot \mathbf{1}_m \mathbf{1}_N^\top$ for small ϵ . This implies

$$G_1(0) \approx -\phi'(0) \cdot W_2^\top Y X^\top.$$

Notice $W_2 \in \mathbb{R}^{K \times m}$ and $Y X^\top \in \mathbb{R}^{K \times N}$, and so $W_2^\top Y X^\top$ is (at most) rank- K . As a result, $G_1(0)$ is approximately (at most) rank- K , with a $\Theta(\epsilon)$ the approximation error. Therefore, one can show

$$\sigma_i(G_1(0)) = \begin{cases} \Theta(\sigma_i(W_2^\top Y X^\top)) \pm \Theta(\epsilon) & i \leq K \\ \Theta(\epsilon) & i > K \end{cases}.$$

Identifying a small-update subspace. We then identify a p -dimensional subspace where $G_1(t)$ has a small component, which is analogous to the subspace identified in Yaras et al. (2023, 2024) for deep linear networks. Let $L_{1,1}(t) \in \mathbb{R}^{m \times K}$ denote the top- K left singular subspace of $G_1(t)$, and $R_{1,2}(t) \in \mathbb{R}^{d \times (d-K)}$ the bottom $d - K$ right singular subspace. We show that $G_1(t)$ has a bounded component in the following p -dimensional subspace \mathcal{S}_{small} :

$$\mathcal{S}_{small} = \mathcal{R}(R_{1,2}(0)) \cap \mathcal{R}^\perp(W_1^\top(0)L_{1,1}(0)/\epsilon). \quad (5)$$

Letting V_2 be an orthonormal basis for \mathcal{S}_{small} , we show $\|G_1(t)V_2\|_F$ and $\|G_1^\top(t)W_1(0)V_2/\epsilon\|_F$ are bounded based on the distances between $\mathcal{R}(R_{1,1}(t))$ and $\mathcal{R}(R_{1,1}(0))$, as well as $\mathcal{R}(L_{1,1}(t))$ and $\mathcal{R}(L_{1,1}(0))$. The $C_1\epsilon$ term in $\rho(t)$ comes from the first GD step, i.e., from $\|G_1(0)V\|_F$ and $\|G_1^\top(0)W_1(0)V_2/\epsilon\|_F$, while the second term in $\rho(t)$ comes from all subsequent steps.

4 Empirical Observations Beyond Theory

In this section, we investigate if low-rank training dynamics persist beyond our theoretical setting in Section 3. We ran all experiments in PyTorch using an NVIDIA A100 GPU.

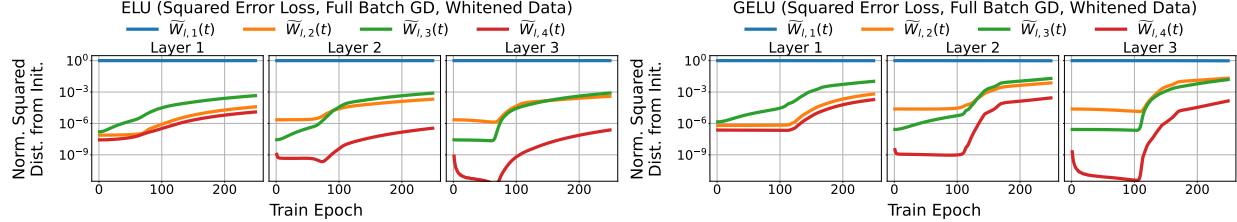


Figure 4: For every $l \in [L - 1]$ in deep MLPs with smooth activations, $\tilde{W}_{l,1}(t)$ accounts for almost all of the change in $\tilde{W}_l(t)$.

4.1 Deeper Networks

Here, we show that low-rank training GD updates emerge in deeper MLPs, where each layer l has a corresponding “small-update subspace” $\mathcal{S}_{small}^{(l)}$. We are interested in identifying if the weight matrices are mostly updated in low-dimensional subspaces. Since $W_L \in \mathbb{R}^{K \times m}$, where $K \ll d \leq m$, we focus our attention to the first $L - 1$ layers, where $W_1 \in \mathbb{R}^{m \times d}$ and $W_l \in \mathbb{R}^{m \times m}$ for $l = 2, \dots, L - 1$.

Network architecture and training. We considered $L = 4$ layer networks with activations $\phi = \text{ELU}$ and GELU. We trained the networks on squared-error loss using full-batch GD, and initialized the first 3 layers to be ϵ -scaled (semi-)orthogonal matrices with $\epsilon = 0.1$. We trained on synthetic data as described in Appendix A.2, and defer remaining details to Appendix A.3.

Small-update subspaces for deeper layers. Recall from (5), the “small update subspace” for the first layer in a two-layer network is

$$\mathcal{S}_{small}^{(1)} = \mathcal{R}(R_{1,2}(0)) \cap \mathcal{R}^\perp(W_1^\top(0)L_{1,1}(0)/\epsilon). \quad (6)$$

Let $V_{1,2} \in \mathbb{R}^{d \times p}$ be an orthonormal basis for $\mathcal{S}_{small}^{(1)}$, and $U_{1,2} := W_1(0)V_{1,2}/\epsilon \in \mathbb{R}^{m \times p}$. Inspired by [Yaras et al. \(2023, 2024\)](#), we define corresponding $V_{l,2}$ and $U_{l,2}$ in W_l for $l = 2, \dots, L - 1$ as follows:

$$V_{l,2} = U_{l-1,2} \quad \text{and} \quad U_{l,2} = W_l(0)V_{l,2}/\epsilon, \quad (7)$$

assuming $W_l(0)$ is initialized as an ϵ -scaled semi-orthogonal matrix. Equivalently,

$$V_{l,2} = W_{l-1}(0)W_{l-2}(0) \cdots W_1(0)V_{1,2}/\epsilon^{l-1} \quad \text{and} \quad U_{l,2} = W_l(0)W_{l-1}(0)W_{l-2}(0) \cdots W_1(0)V_{1,2}/\epsilon^l. \quad (8)$$

Define $V_l := [V_{l,1} \ V_{l,2}] \in \mathbb{R}^{m \times m}$ and $U_l := [U_{l,1} \ U_{l,2}] \in \mathbb{R}^{m \times m}$, where $V_{l,1} \in \mathbb{R}^{m \times (m-p)}$ and $U_{l,1} \in \mathbb{R}^{m \times (m-p)}$ are orthogonal to $V_{l,2}$ and $U_{l,2}$. Finally, let

$$\tilde{W}_l(t) = \begin{bmatrix} U_{l,1}^\top W_l(t) V_{l,1} & U_{l,1}^\top W_l(t) V_{l,2} \\ U_{l,2}^\top W_l(t) V_{l,1} & U_{l,2}^\top W_l(t) V_{l,2} \end{bmatrix} := \begin{bmatrix} \tilde{W}_{l,1}(t) & \tilde{W}_{l,2}(t) \\ \tilde{W}_{l,3}(t) & \tilde{W}_{l,4}(t) \end{bmatrix} \in \mathbb{R}^{m \times m}, \quad (9)$$

which implies $W_l(t) = U_l \tilde{W}_l(t) V_l^\top$. Note $\tilde{W}_{l,1}(t) \in \mathbb{R}^{(m-p) \times (m-p)}$, $\tilde{W}_{l,2}(t) \in \mathbb{R}^{(m-p) \times p}$, $\tilde{W}_{l,3}(t) \in \mathbb{R}^{p \times (m-p)}$, and $\tilde{W}_{l,4}(t) \in \mathbb{R}^{p \times p}$.

Results. We plot the normalized squared distance of each $\tilde{W}_{l,i}(t)$ from their initializations, i.e., $\|\tilde{W}_{l,i}(t) - \tilde{W}_{l,i}(0)\|_F^2 / \|\tilde{W}_l(t) - \tilde{W}_l(0)\|_F^2$. The results are shown in Figure 4, averaged over 10 trials. For all $l \in [L - 1]$, $\tilde{W}_{l,1}(t)$ again accounts for most of the changes in $\tilde{W}_l(t)$, and thus $W_l(t)$ themselves. This implies the **GD updates of the deeper layers are also concentrated within low-dimensional subspaces**.

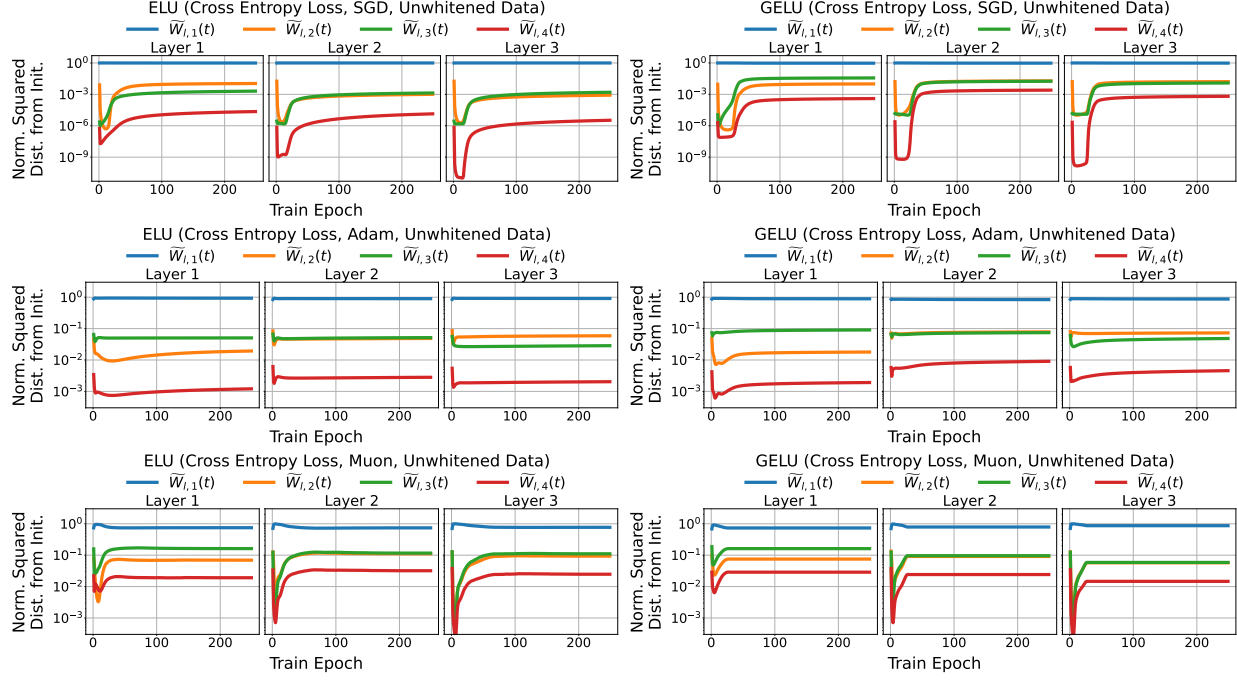


Figure 5: Training deep MLPs with SGD plus momentum (top row), or with Adam (bottom row), on unwhitened input data using cross-entropy loss approximately maintains the previously observed low-rank training dynamics.

4.2 Loss Function, Optimizer, and Unwhitened Data

Next, we investigate the impact of the loss function, optimizer, and unwhitened data. Thus far, we have been training MLPs using full batch GD on squared-error loss with whitened input data. Here, we generated X as described in Appendix A.2, but did not whiten X . We also trained the networks using 1) minibatch SGD with momentum, 2) Adam, and 3) Muon, all on cross-entropy loss; we again defer specific experimental details to Appendix A.3.

Figure 5 again shows the normalized squared distance of each $\widetilde{W}_{l,i}(t)$ from their initializations. Once again, $\widetilde{W}_{l,1}(t)$ accounts for a majority of the change in $\widetilde{W}_l(t)$, and thus $W_l(t)$, albeit less so when trained with Adam and Muon. Regardless, this implies the low-rank training phenomenon approximately holds in more realistic training settings.

5 Low-Rank Parameterization in MLPs

From Sections 3 and 4, in an MLP with smooth activation functions, we find each weight matrix is mostly updated within a layer-dependent $2K$ -dimensional subspace. Based on these insights, we find there exists a **low-rank parameterization** that, when initialized properly, achieves *near-equivalent* performance compared to their fully parameterized counterpart. For some width parameter r , we refer to the following parameterization as a **low-rank MLP**:

$$W_L \phi \left(\widetilde{U} \widetilde{W}_{L-1} \phi \left(\widetilde{W}_{L-2} \dots \widetilde{W}_2 \phi \left(\widetilde{W}_1 \widetilde{V}^\top X \right) \dots \right) \right), \quad (10)$$

where $W_L \in \mathbb{R}^{K \times m}$, $\widetilde{U} \in \mathbb{R}^{m \times r}$, $\widetilde{V} \in \mathbb{R}^{d \times r}$ and $\widetilde{W}_l \in \mathbb{R}^{r \times r}$ for $l \in [L-1]$.

Initializing and training \widetilde{U} and \widetilde{V} . For ease of exposition, suppose $m = d$, so $m - p = d - (d - 2K) = 2K$. In this case, from Section 4, we observe each layer is updated in a $2K$ -dimensional subspace, where each layer's subspace is defined from (8). Thus, setting $r = 2K$, and initializing $W_l(0)$ as ϵ -scaled orthogonal matrices for

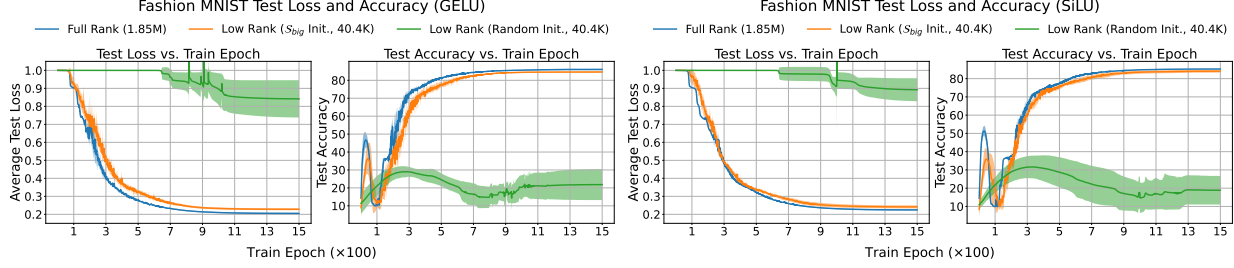


Figure 6: The properly-initialized low-rank MLP (orange) achieves nearly-identical test loss and accuracy trajectories as the fully parameterized MLP (blue). Meanwhile, the low-rank MLP with random subspace initialization (green) gets stuck at a noticeably worse local minimum.

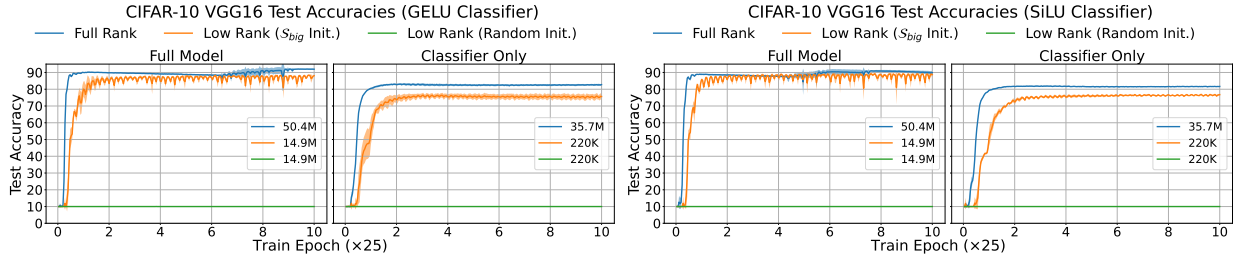


Figure 7: The properly-initialized low-rank MLP classifier head (orange) achieves similar test accuracies to the fully parameterized version (blue) in VGG-16 on CIFAR-10, while the random-subspace initialized low-rank MLP (green) is stuck in the random guessing stage.

all $l \in [L-1]$, we find \tilde{U} and \tilde{V} should be initialized as follows. Recall $\mathcal{S}_{small}^{(1)}$ in (6), and denote its orthogonal complement as $\mathcal{S}_{big}^{(1)}$. We initialize $\tilde{V} \in \mathbb{R}^{d \times 2K}$ as an orthonormal basis of $\mathcal{S}_{big}^{(1)}$, and then initialize \tilde{U} according to (8), i.e., $\tilde{U} = W_{L-1}(0) \cdots W_1(0) \tilde{V} / \epsilon^{L-1} \in \mathbb{R}^{d \times 2K}$. We call this the “ **S_{big} initialization**”, which we find to be critical to its performance. After initialization, we train \tilde{U} and \tilde{V} using the same learning rate as \tilde{W}_l .

5.1 Experiments

In this section, we provide empirical evidence showing that, when \tilde{U} and \tilde{V} are properly initialized, **the low-rank MLP achieves near-equivalent performance** (test loss and/or accuracy) **compared to the fully parameterized MLP**, assuming the hyperparameters remain the same when training the two types of networks. We again ran all experiments in PyTorch using an NVIDIA A100 GPU.

We emphasize that the goal of these experiments is not necessarily to find optimal hyperparameters to maximize performance. Rather, we aim to show that, for a given MLP that is trained using some (possibly sub-optimal) training algorithm and hyperparameters, there exists a low-rank MLP that achieves similar performance if initialized properly.

5.1.1 Fashion MNIST using MLPs

We trained fully parameterized and low-rank MLPs on Fashion MNIST (Xiao et al., 2017). We pre-processed all images by re-scaling the pixel values to lie in $[0, 1]$, and then normalized them to have zero mean and unit variance.

Network architecture and training. We used $L = 4$ layer networks with GELU and SiLU activations, setting $m = d = 784$ and $r = 2K$. We initialized each W_l and \tilde{W}_l as ϵ -scaled (semi-)orthogonal matrices, with $\epsilon = 0.1$. We initialized \tilde{U} and \tilde{V} in two different ways: 1) the S_{big} initialization scheme, and 2) as random semi-orthogonal matrices. We trained all networks on all $N = 5 \times 10^4$ training images for $T = 1500$ epochs

using full-batch GD on (total) squared-error loss, which aligns with the training algorithm in our theoretical setting. Since this is a classification setting, we used one-hot encoded labels. Finally, we set $\eta = 10^{-5}$ and used a cosine annealing scheduler.

Results. Figure 6 shows the test losses and accuracies for the fully parameterized and low-rank MLPs, averaged over 5 trials. Note that we trained the networks using vanilla full-batch GD, so all networks (likely) converged to local minima. Nevertheless, keeping the training algorithm and hyperparameters fixed between the two parameterizations, the low-rank MLP with \mathcal{S}_{big} initialization achieves nearly identical performance to the fully parameterized MLP. Meanwhile, the low-rank MLP with random subspace initialization gets stuck in a much worse local minimum. We provide an ablation study on the initialization of \tilde{U} and \tilde{V} in Appendix F.1.

5.1.2 CIFAR-10 using VGG-16

Here, we train a modified version of VGG-16 (Simonyan and Zisserman, 2014) on CIFAR-10 (Krizhevsky et al., 2009). We pre-processed each image the same way as in Section 5.1.1, but after re-sizing the images to be of size $224 \times 224 \times 3$ using bilinear interpolation.

Network architecture. We used modified VGG-16 models (Simonyan and Zisserman, 2014). The original model contains a convolutional network as a feature extractor, and then $L = 3$ layer ReLU MLP classifier head. Due to limited computational resources, we reduced the final average pooling layer size from 7×7 to 3×3 , and thus changed the input dimension of the classifier head from $512 \times 7 \times 7$ to $512 \times 3 \times 3$. This reduced the full model size from about 138M parameters to about 50M. We also replaced the ReLU in the original classifier head with GELU and SiLU.

Training. In all experiments, we initialized the convolutional layers using ImageNet pre-trained weights, and initialized W_l and \tilde{W}_l in the classifier head in the same manner as in Section 5.1.1, again with $r = 2K$. To initialize \tilde{U} and \tilde{V} , and used 1) an (unbiased) estimator of the first MLP-layer gradient via a random batch of 128 images to estimate $\mathcal{S}_{big}^{(1)}$, and 2) random semi-orthogonal matrices. For all model types, we conducted two training paradigms:

1. **Full model training.** We fine-tuned the convolutional layers from the ImageNet pre-trained weights, in addition to training the classifier head from initialization.
2. **Classifier-only training.** We kept the convolutional layers frozen at the ImageNet pre-trained weights, and only trained the classifier head from initialization.

We trained all models on cross-entropy loss using SGD with momentum for 250 epochs. We set $\eta = 5 \times 10^{-3}$ with a cosine annealing scheduler, the batch size to 128, the momentum to 0.9, and weight decay to 5×10^{-4} .

Results. Figure 7 shows the test accuracies of VGG-16 with the fully-parameterized and low-rank classifier heads, again averaged over 5 trials. Under full model training, VGG-16 with the low-rank MLP and \mathcal{S}_{big} initialization consistently achieved very similar test accuracy to the corresponding model with the fully parameterized MLP. Meanwhile, using the same training hyperparameters, the VGG-16 with random-subspace initialized MLP did not escape the random guessing stage.

When we only trained the classifier head, there was a noticeable gap in test accuracy (about 5% – 10%) between the low-rank MLP with \mathcal{S}_{big} initialization and the fully parameterized version. In Appendix F.2, we observe setting the width $r = 4K$ noticeably closes this gap. We also note the low-rank MLP with random \tilde{U}, \tilde{V} initialization again did not escape the random guessing stage.

Finally, the model with the low-rank classifier head took noticeably more epochs to (nearly) match the performance of the fully parameterized version. We believe this is because we initialized \tilde{V} and \tilde{U} using an estimate of $\mathcal{S}_{big}^{(1)}$ via a minibatch of data, rather than using all of the data samples to determine the true $\mathcal{S}_{big}^{(1)}$.

6 Related Work

In this section, we provide more detailed discussions on related works.

6.1 Low-Dimensional Learning in Neural Networks

A recent line of empirical work has shown the GD and SGD dynamics of deep neural networks (DNNs) occur within a small subset of the full parameter space. Specifically, [Li et al. \(2018, 2022\)](#); [Larsen et al. \(2022\)](#) observed DNNs can be trained in low-dimensional subspaces of the parameter space. Our work is similar to these works, since we observe and prove a similar phenomenon in MLP architectures. The main difference is [Li et al. \(2018\)](#); [Larsen et al. \(2022\)](#) showed low-dimensional training is *possible* in *random* subspaces, and [Li et al. \(2022\)](#) determined the subspace to train in via the full-parameter training trajectory of an initial training phase. Meanwhile, in our work, we show the weights are *naturally* trained within low-dimensional subspaces that depend on the weights and first-layer gradient *at initialization* of the fully parameterized MLP. Identifying these subspaces only requires a single forward and backward pass, and so no training is needed to find the optimization subspaces in our work.

Similarly, [Frankle and Carbin \(2019\)](#) proposed the lottery ticket hypothesis: dense, randomly initialized neural networks contain sparse sub-networks that, if trained separately, achieve similar performance to the full network in similar training time. Again, our work is similar in that we find a “low-rank lottery ticket” in MLP architectures. The main difference is that in [Frankle and Carbin \(2019\)](#), although the sparse winning lottery tickets emerge at random initialization, *identifying* these lottery tickets requires an initial training and pruning phase in the full parameter space. In our work, the “low-rank lottery ticket” in MLPs can be completely identified at initialization of the original network, again with only a single forward and backward pass.

Finally, there is a rich line of literature on the emergence of low-rank structure in matrix factorization ([Gunasekar et al., 2017](#); [Li et al., 2021](#)) and deep linear networks ([Arora et al., 2019](#); [Gidel et al., 2019](#); [Yaras et al., 2023, 2024](#); [Kwon et al., 2024](#)); see [Vardi \(2023\)](#) for a survey. As mentioned in Section 1, among these works, [Yaras et al. \(2023, 2024\)](#); [Kwon et al. \(2024\)](#) are most closely related to ours. They theoretically proved that when deep linear networks are trained via GD, each weight matrix is updated in an unchanging low-dimensional subspace that is determined at initialization. This subspace is also dependent on the weights and the first-layer gradient at initialization. [Yaras et al. \(2023\)](#) proved this in a setting with whitened input data, while [Yaras et al. \(2024\)](#); [Kwon et al. \(2024\)](#) focused on deep matrix factorization (i.e., no input data). This work is largely inspired by the findings of [Yaras et al. \(2023\)](#), as we extend the investigation to nonlinear MLP architectures.

6.2 Low Rank Gradients in Neural Networks

Another line of work studied the emergence of low-rank gradients in deep neural networks. In particular, [Gur-Ari et al. \(2018\)](#) empirically observed the gradients become well-aligned with the corresponding Hessian’s top eigenspace, which remains approximately constant throughout long training periods. Furthermore, [Ba et al. \(2022\)](#); [Zhao et al. \(2024\)](#); [Jaiswal et al. \(2025\)](#); [Sonthalia et al. \(2025\)](#) theoretically analyzed the emergence of low-rank gradients in nonlinear networks. For instance, [Ba et al. \(2022\)](#) showed under a student-teacher model with Gaussian input data and scalar outputs, the gradient of the first layer in a two-layer nonlinear network is approximately rank-1. Likewise, under the same network assumptions but with more relaxed data assumptions, [Sonthalia et al. \(2025\)](#) showed the gradient is approximately rank two. In a related direction, [Zhao et al. \(2024\)](#); [Jaiswal et al. \(2025\)](#) studied the low-rank property of the gradients of *reversible* neural networks. Specifically, [Zhao et al. \(2024\)](#) provided upper bounds on the gradient stable ranks in reversible networks, while [Jaiswal et al. \(2025\)](#) showed the gradients asymptotically align with the top eigenspace of their corresponding Hessians, in line with the observations of [Gur-Ari et al. \(2018\)](#). Our work is related to the emergence of low-rank gradients in the following way. In Theorem 3.5, we show that the upper bound on the change in the perturbation terms of $\bar{W}_1(t)$ depends on the gradient’s $(K + 1)^{th}$ singular value. The low-rank GD dynamics in $W_1(t)$ relies on the gradient being approximately rank- K .

6.3 Implicit Bias in Two-Layer Networks

Finally, several other works studied the implicit bias of gradient flow (GF) and GD towards low-rank weights in two-layer nonlinear networks. For example, [Frei et al. \(2023\)](#); [Kou et al. \(2023\)](#) showed when two-layer ReLU and Leaky-ReLU networks are trained using GF or GD, the first-layer weights have a bounded stable rank at convergence. [Min et al. \(2024\)](#) showed a similar result in ReLU networks for orthogonally separable data. Our analysis on two-layer networks differs from these works, since we show *each GD update* of the first-layer weights mostly occurs in a low-dimensional subspace. Meanwhile, these works focus on the low-rankness of the first-layer weights *at convergence*.

7 Conclusion

In this work, we investigated when low-rank training dynamics emerge in nonlinear networks, using MLP architectures as a case study. We showed that in MLPs with smooth activation functions, the training dynamics are highly concentrated within invariant low-dimensional subspaces. We provided theoretical insight into this phenomenon on two-layer networks trained with GD, and our experiments show the phenomenon holds beyond our theoretical setting. From these insights, we empirically showed there exists a low-rank MLP parameterization that, if initialized in the proper subspaces, nearly matches the classification accuracy of the fully parameterized version.

Acknowledgements

QQ and AX acknowledge support from NSF CAREER CCF-2143904, NSF IIS-2312842, NSF IIS-2402950, NSF CCSS-2532643, and a Google Research Scholar Award. LB and CY acknowledge support from NSF CCF-2331590, NSF CAREER CCF-1845076, and an Intel early career award.

References

George Andriopoulos, Zixuan Dong, Li Guo, Zifan Zhao, and Keith Ross. The prevalence of neural collapse in neural multivariate regression. *Advances in Neural Information Processing Systems*, 37:126417–126451, 2024.

Sanjeev Arora, Nadav Cohen, Noah Golowich, and Wei Hu. A convergence analysis of gradient descent for deep linear neural networks. In *International Conference on Learning Representations*, 2019.

Jimmy Ba, Murat A Erdogdu, Taiji Suzuki, Zhichao Wang, Denny Wu, and Greg Yang. High-dimensional asymptotics of feature learning: How one gradient step improves the representation. *Advances in Neural Information Processing Systems*, 35:37932–37946, 2022.

Laura Balzano, Tianjiao Ding, Benjamin D Haeffele, Soo Min Kwon, Qing Qu, Peng Wang, Zhangyang Wang, and Can Yaras. An overview of low-rank structures in the training and adaptation of large models. *arXiv preprint arXiv:2503.19859*, 2025.

Yajie Bao, Amarda Shehu, and Mingrui Liu. Global convergence analysis of local sgd for two-layer neural network without overparameterization. *Advances in Neural Information Processing Systems*, 36:24610–24660, 2023.

Dimitri P Bertsekas. Nonlinear programming. *Journal of the Operational Research Society*, 48(3):334–334, 1997.

Etienne Boursier, Lucas Pillaud-Vivien, and Nicolas Flammarion. Gradient flow dynamics of shallow relu networks for square loss and orthogonal inputs. *Advances in Neural Information Processing Systems*, 35: 20105–20118, 2022.

Lukas Braun, Clémentine Dominé, James Fitzgerald, and Andrew Saxe. Exact learning dynamics of deep linear networks with prior knowledge. *Advances in Neural Information Processing Systems*, 35:6615–6629, 2022.

Dmitry Chistikov, Matthias Englert, and Ranko Lazic. Learning a neuron by a shallow relu network: Dynamics and implicit bias for correlated inputs. *Advances in Neural Information Processing Systems*, 36:23748–23760, 2023.

Clémentine Carla Juliette Dominé, Nicolas Anguita, Alexandra Maria Proca, Lukas Braun, Daniel Kunin, Pedro AM Mediano, and Andrew M Saxe. From lazy to rich: Exact learning dynamics in deep linear networks. In *The Thirteenth International Conference on Learning Representations*, 2025.

Jonathan Frankle and Michael Carbin. The lottery ticket hypothesis: Finding sparse, trainable neural networks. In *International Conference on Learning Representations*, 2019.

Spencer Frei, Gal Vardi, Peter Bartlett, Nathan Srebro, and Wei Hu. Implicit bias in leaky relu networks trained on high-dimensional data. In *International Conference on Learning Representations*, 2023.

Gauthier Gidel, Francis Bach, and Simon Lacoste-Julien. Implicit regularization of discrete gradient dynamics in linear neural networks. *Advances in Neural Information Processing Systems*, 32, 2019.

Pulkit Gopalani and Anirbit Mukherjee. Global convergence of sgd on two layer neural nets. *Information and Inference: A Journal of the IMA*, 14(1):iaae035, 2025.

Suriya Gunasekar, Blake E Woodworth, Srinadh Bhojanapalli, Behnam Neyshabur, and Nati Srebro. Implicit regularization in matrix factorization. *Advances in neural information processing systems*, 30, 2017.

Guy Gur-Ari, Daniel A Roberts, and Ethan Dyer. Gradient descent happens in a tiny subspace. *arXiv preprint arXiv:1812.04754*, 2018.

Roger A Horn and Charles R Johnson. *Matrix analysis*. Cambridge university press, 2012.

Edward J Hu, Phillip Wallis, Zeyuan Allen-Zhu, Yuanzhi Li, Shean Wang, Lu Wang, Weizhu Chen, et al. Lora: Low-rank adaptation of large language models. In *International Conference on Learning Representations*, 2022.

Like Hui and Mikhail Belkin. Evaluation of neural architectures trained with square loss vs. cross-entropy in classification tasks. In *The International Conference on Learning Representations*, 2021.

Ajay Jumar Jaiswal, Yifan Wang, Lu Yin, Shiwei Liu, Runjin Chen, Jiawei Zhao, Ananth Grama, Yuandong Tian, and Zhangyang Wang. From low rank gradient subspace stabilization to low-rank weights: Observations, theories, and applications. In *International Conference on Machine Learning*, 2025.

Yiwen Kou, Zixiang Chen, and Quanquan Gu. Implicit bias of gradient descent for two-layer relu and leaky relu networks on nearly-orthogonal data. *Advances in Neural Information Processing Systems*, 36:30167–30221, 2023.

Alex Krizhevsky, Geoffrey Hinton, et al. Learning multiple layers of features from tiny images. 2009.

Soo Min Kwon, Zekai Zhang, Dogyoon Song, Laura Balzano, and Qing Qu. Efficient low-dimensional compression of overparameterized models. In *International Conference on Artificial Intelligence and Statistics*, pages 1009–1017. PMLR, 2024.

Brett W Larsen, Stanislav Fort, Nic Becker, and Surya Ganguli. How many degrees of freedom do we need to train deep networks: a loss landscape perspective. In *International Conference on Learning Representations*, 2022.

Chunyuan Li, Heerad Farkhoor, Rosanne Liu, and Jason Yosinski. Measuring the intrinsic dimension of objective landscapes. In *International Conference on Learning Representations*, 2018.

Tao Li, Lei Tan, Zhehao Huang, Qinghua Tao, Yipeng Liu, and Xiaolin Huang. Low dimensional trajectory hypothesis is true: Dnns can be trained in tiny subspaces. *IEEE Transactions on Pattern Analysis and Machine Intelligence*, 45(3):3411–3420, 2022.

Zhiyuan Li, Yuping Luo, and Kaifeng Lyu. Towards resolving the implicit bias of gradient descent for matrix factorization: Greedy low-rank learning. In *International Conference on Learning Representations*, 2021.

Hancheng Min, Enrique Mallada, and Rene Vidal. Early neuron alignment in two-layer relu networks with small initialization. In *The Twelfth International Conference on Learning Representations*, 2024.

Samet Oymak and Mahdi Soltanolkotabi. Overparameterized nonlinear learning: Gradient descent takes the shortest path? In *International Conference on Machine Learning*, pages 4951–4960. PMLR, 2019.

Samet Oymak and Mahdi Soltanolkotabi. Toward moderate overparameterization: Global convergence guarantees for training shallow neural networks. *IEEE Journal on Selected Areas in Information Theory*, 1(1):84–105, 2020.

Vardan Papyan, XY Han, and David L Donoho. Prevalence of neural collapse during the terminal phase of deep learning training. *Proceedings of the National Academy of Sciences*, 117(40):24652–24663, 2020.

Sahar Rajabi, Nayeema Nonta, and Sirisha Rambhatla. Subtrack++: Gradient subspace tracking for scalable llm training. *Advances in Neural Information Processing Systems*, 38, 2025.

Thomas Robert, Mher Safaryan, Ionut-Vlad Modoranu, and Dan Alistarh. Ldadam: Adaptive optimization from low-dimensional gradient statistics. In *The Thirteenth International Conference on Learning Representations*, 2025.

Steffen Schotthöfer, Emanuele Zangrando, Jonas Kusch, Gianluca Ceruti, and Francesco Tudisco. Low-rank lottery tickets: finding efficient low-rank neural networks via matrix differential equations. *Advances in Neural Information Processing Systems*, 35:20051–20063, 2022.

Karen Simonyan and Andrew Zisserman. Very deep convolutional networks for large-scale image recognition. *arXiv preprint arXiv:1409.1556*, 2014.

Rishi Sonthalia, Michael Murray, and Guido Montúfar. Low rank gradients and where to find them. *arXiv preprint arXiv:2510.01303*, 2025.

Michael Spivak. *Calculus*. Cambridge University Press, 2006.

Nadav Timor, Gal Vardi, and Ohad Shamir. Implicit regularization towards rank minimization in relu networks. In *International Conference on Algorithmic Learning Theory*, pages 1429–1459. PMLR, 2023.

Joel A Tropp et al. An introduction to matrix concentration inequalities. *Foundations and Trends® in Machine Learning*, 8(1-2):1–230, 2015.

Gal Vardi. On the implicit bias in deep-learning algorithms. *Communications of the ACM*, 66(6):86–93, 2023.

Peng Wang, Xiao Li, Can Yaras, Zhihui Zhu, Laura Balzano, Wei Hu, and Qing Qu. Understanding deep representation learning via layerwise feature compression and discrimination. *arXiv preprint arXiv:2311.02960*, 2023.

Per-Åke Wedin. Perturbation bounds in connection with singular value decomposition. *BIT Numerical Mathematics*, 12(1):99–111, 1972.

Hermann Weyl. Inequalities between the two kinds of eigenvalues of a linear transformation. *Proceedings of the national academy of sciences*, 35(7):408–411, 1949.

Han Xiao, Kashif Rasul, and Roland Vollgraf. Fashion-mnist: a novel image dataset for benchmarking machine learning algorithms. *arXiv preprint arXiv:1708.07747*, 2017.

Alec S Xu, Can Yaras, Peng Wang, and Qing Qu. Understanding how nonlinear layers create linearly separable features for low-dimensional data. *arXiv preprint arXiv:2501.02364*, 2025.

Can Yaras, Peng Wang, Wei Hu, Zhihui Zhu, Laura Balzano, and Qing Qu. The law of parsimony in gradient descent for learning deep linear networks. *arXiv preprint arXiv:2306.01154*, 2023.

Can Yaras, Peng Wang, Laura Balzano, and Qing Qu. Compressible dynamics in deep overparameterized low-rank learning & adaptation. In *International Conference on Machine Learning*, 2024.

Zhong Zhang, Bang Liu, and Junming Shao. Fine-tuning happens in tiny subspaces: Exploring intrinsic task-specific subspaces of pre-trained language models. In *Proceedings of the 61st Annual Meeting of the Association for Computational Linguistics (Volume 1: Long Papers)*, pages 1701–1713, 2023.

Jiawei Zhao, Zhenyu Zhang, Beidi Chen, Zhangyang Wang, Anima Anandkumar, and Yuandong Tian. Galore: Memory-efficient llm training by gradient low-rank projection. In *International Conference on Machine Learning*, pages 61121–61143. PMLR, 2024.

Jinxin Zhou, Chong You, Xiao Li, Kangning Liu, Sheng Liu, Qing Qu, and Zhihui Zhu. Are all losses created equal: A neural collapse perspective. *Advances in Neural Information Processing Systems*, 35:31697–31710, 2022.

Hanqing Zhu, Zhenyu Zhang, Wenyan Cong, Xi Liu, Sem Park, Vikas Chandra, Bo Long, David Z Pan, Zhangyang Wang, and Jinwon Lee. Apollo: Sgd-like memory, adamw-level performance. *Proceedings of Machine Learning and Systems*, 7, 2025.

A Additional Simulation Details and Results

In this section, we provide additional experimental details and/or results for Figure 1, Section 2.1 (Figure 2), Section 3.2 (Figure 3), and Section 4 (Figures 4 and 5).

A.1 Additional Details and Results for Figure 2

In this section, we provide experimental details and additional results for the experiments introduced in Figure 1 and Section 2.1 (Figure 2).

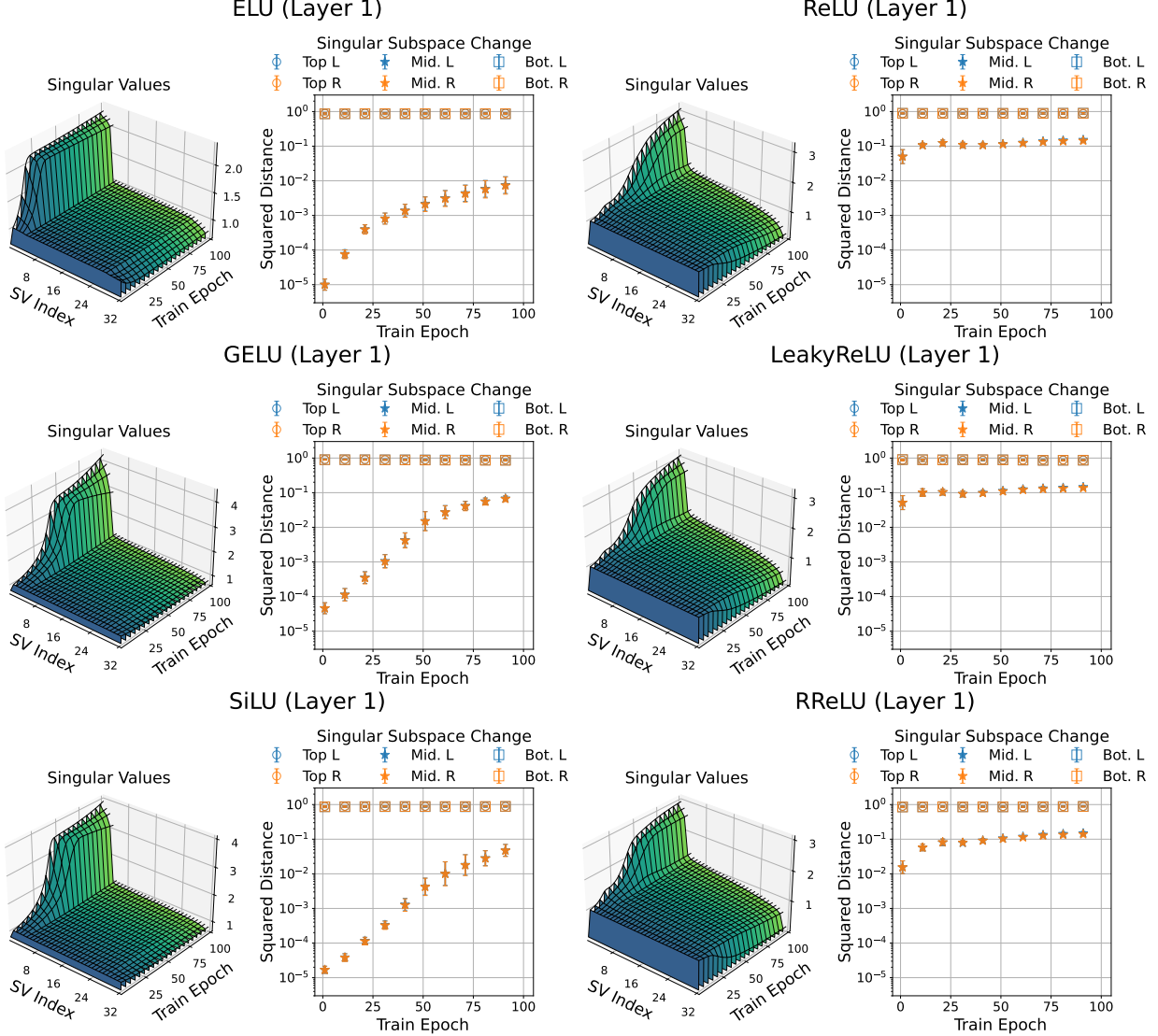


Figure 8: For networks with smooth activation functions, the middle singular subspace of the first layer weights evolves noticeably slower than in networks with non-smooth activation functions.

Data generation. To generate the data, we set $d = 32$, $K = 4$, and $N = 2000$, so $n = N/K = 500$. We generated X from a Gaussian mixture distribution as follows: first, we sampled K means $\mu_k \sim \mathcal{N}(\mathbf{0}_d, I_d)$. Next, for each $k \in [K]$, we generated $n = 500$ samples in the k^{th} class via $x_{k,i} \sim \mathcal{N}(\mu_k, \sigma^2 I_d)$ with $\sigma^2 = 3$.

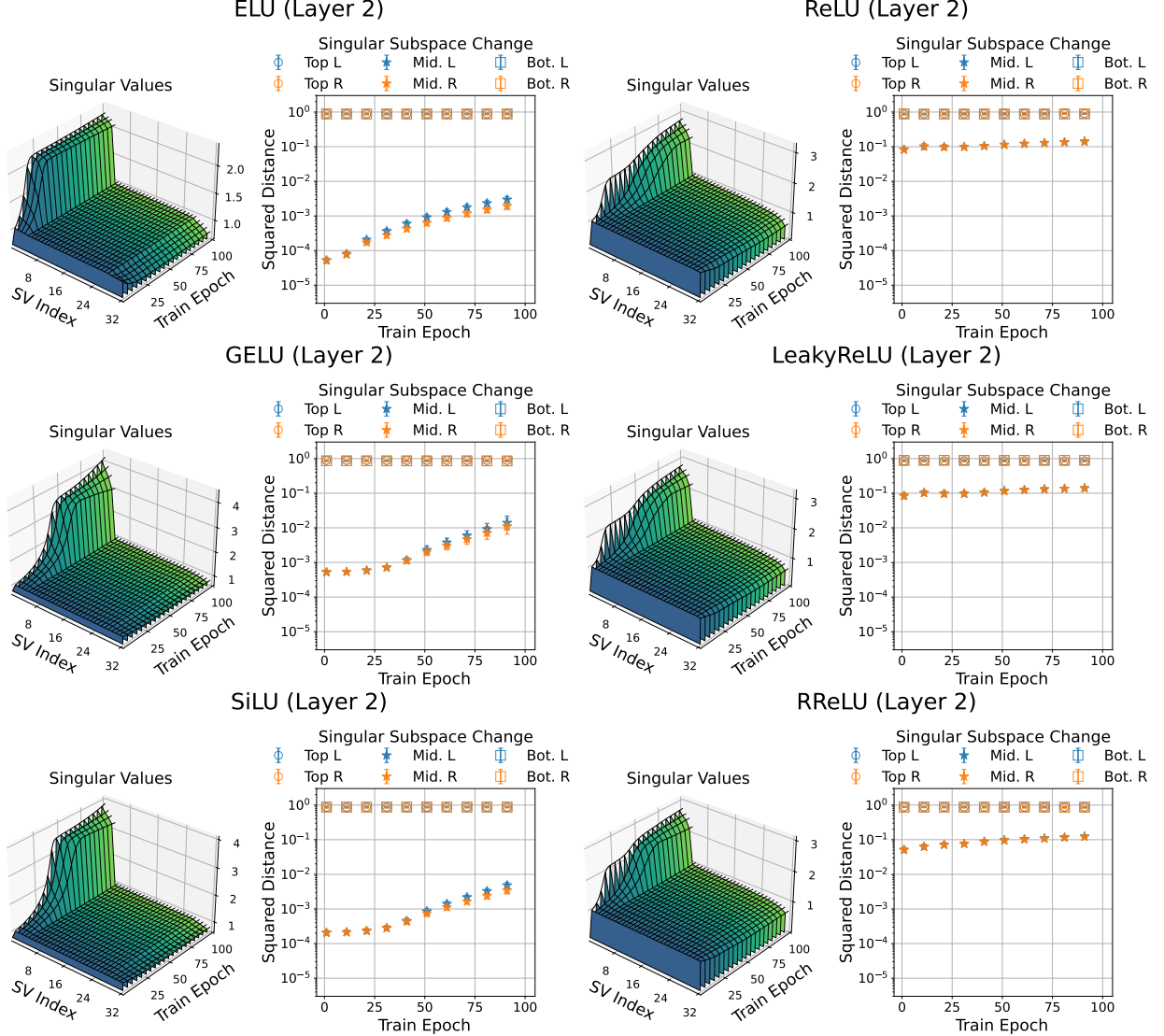


Figure 9: The change in the middle singular subspaces of the second layer weights in networks with smooth vs. nonsmooth activation functions mimic those in the first layer weights (Figure 8).

Then, we set $\mathbf{X} = [x_{1,1} \dots x_{1,n} \dots x_{K,1} \dots x_{K,n}]$. Finally, we pre-processed \mathbf{X} by whitening, e.g., $\mathbf{X}\mathbf{X}^\top = \mathbf{I}_d$. We generated the label matrix \mathbf{Y} via $\mathbf{Y} = \mathbf{I}_K \otimes \mathbf{1}_n$.

Network architectures and training. We considered six different $L = 4$ layer MLPs: three with smooth activation functions ELU, GELU, SiLU, and three with nonsmooth activations ReLU, Leaky-ReLU, and a randomized Leaky-ReLU, called RReLU. For ELU, we set the PyTorch parameter $\alpha = 1$, while for Leaky-ReLU, we set the PyTorch slope parameter $\alpha = 0.01$. In all networks, we set $m = d = 32$, and initialized all the weight matrices as ϵ -scaled orthogonal matrices, with $\epsilon = 1$.

Let $\mathbf{W}_l(t) = [A_{l,1}(t) \ A_{l,2}(t) \ A_{l,3}(t)] \begin{bmatrix} S_{l,1}(t) & & \\ & S_{l,2}(t) & \\ & & S_{l,3}(t) \end{bmatrix} [B_{l,1}(t) \ B_{l,2}(t) \ B_{l,3}(t)]^\top$ be an SVD of $\mathbf{W}_l(t)$, where $A_{l,1}(t)S_{l,1}(t)B_{l,1}^\top(t)$, $A_{l,2}(t)S_{l,2}(t)B_{l,2}^\top(t)$, and $A_{l,3}(t)S_{l,3}(t)B_{l,3}^\top(t)$ respectively denote the top- K , middle $d - 2K$, and bottom- K SVD components. We tracked the change in top and bottom- K left singular

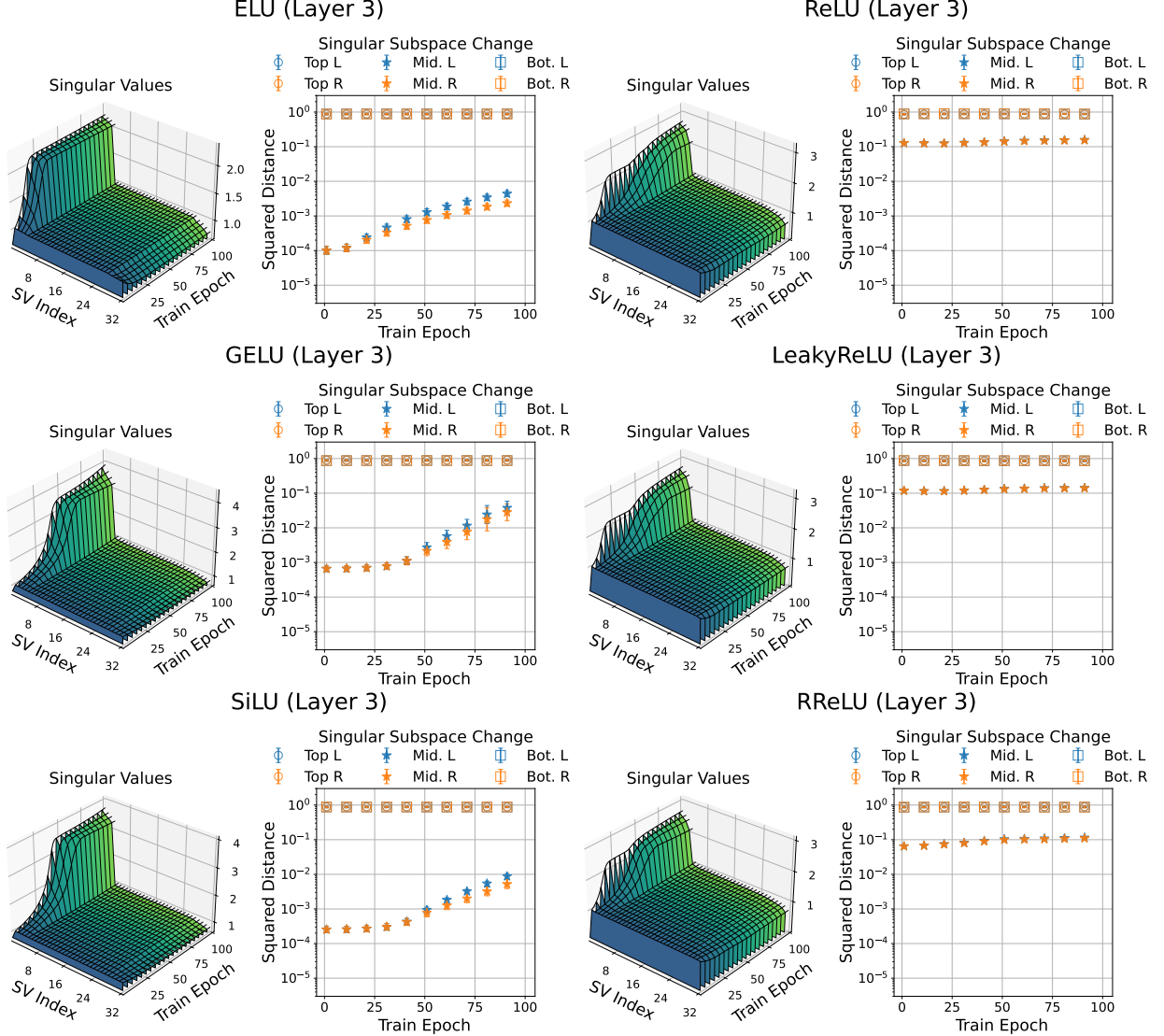


Figure 10: The change in the middle singular subspaces of the third layer weights in networks with smooth vs. nonsmooth activation functions mimic those in the first and second layer weights (Figures 8 and 9).

subspaces via

$$\|\sin \Theta (A_{l,1}(t), A_{l,1}(0))\|_2^2 \quad \text{and} \quad \|\sin \Theta (A_{l,3}(t), A_{l,3}(0))\|_2^2,$$

and similarly for the top and bottom- K right singular subspaces, where $\|\sin \Theta (\mathbf{U}_1, \mathbf{U}_2)\|_2$ is defined in Definition 3.1 for $\mathbf{U}_1, \mathbf{U}_2$ with orthonormal columns. For the middle $d - 2K$ singular subspaces, we computed

$$\|\sin \Theta (A_{l,2}(t), \mathbf{U}_{l,2})\|_F^2 \quad \text{and} \quad \|\sin \Theta (B_{l,2}(t), V_{l,2})\|_F^2,$$

where $\mathbf{U}_{l,2}$ and $V_{l,2}$ are defined in Equation (8).

Additional results. Figures 8 to 10 shows the same results as in Figure 2, but with all nonlinear activations and layers. The behavior in the MLPs with smooth activations is similar to that of the ELU network in Figure 2, while the MLPs with nonsmooth activations behave similarly to that of the ReLU network in Figure 2. This supports our conjecture that smooth activations encourage lower-rank training dynamics in MLPs.

A.2 Experimental Details for Figure 3

Here, we provide additional details on the experimental setup to generate Figure 3. All experiments were run in PyTorch using an NVIDIA A100 GPU.

Data generation. We set $d = 64$, $N = 1000$, and $K = 4$. Under these parameters, we generated the data as described in Appendix A.1.

Network architecture and training. We trained W_1 only in a two-layer neural network $f_{W_1}(X) = W_2\phi(W_1X)$ with $m = 72$ on squared error loss (4) using full-batch GD (3) with $\eta = 10^{-2}$. We considered $\phi = \text{ELU}$, GELU , and SiLU , which are all smooth. We initialized $W_1 \in \mathbb{R}^{m \times d}$ to be an ϵ -scaled semi-orthogonal matrix sampled uniformly at random, with $\epsilon = 10^{-2}$, and then set W_2 to have frozen iid uniform entries between -1 and 1 .

A.3 Experimental Details for Section 4

In this section, we provide additional experimental details for Section 4.

Data generation. In Sections 4.1 and 4.2 (Figures 4 and 5 respectively), we adhered to the exact same data generation process as in Appendix A.1, but we skipped the whitening pre-processing step on X in Section 4.2 (Figure 5).

Network architecture and training. We considered $L = 4$ layer networks of width $m = 72$ with activations $\phi = \text{ELU}$ and GELU . We initialized the first 3 layers to be ϵ -scaled (semi-)orthogonal matrices with $\epsilon = 0.1$, and the last layer W_L with iid uniform entries between -1 and 1 .

In Section 4.1 (Figure 4), we trained the network on squared-error loss using full-batch GD for 250 epochs. For the ELU network, we set $\eta = 10^{-3}$, while for the GELU network, we set $\eta = 5 \times 10^{-3}$. Meanwhile, in Section 4.2 (Figure 5), we trained the networks using 1) SGD with momentum, 2) Adam, and 3) Muon. For SGD and Muon, we set the momentum to 0.9, while for Adam, we used the default PyTorch parameters. For all optimizers, we set the batch size to 32, $\eta = 10^{-4}$ for the ELU network, and $\eta = 5 \times 10^{-4}$ for GELU.

B Why Activation Smoothness Matters: Some Intuition

From Figure 2, we observed that compared to MLPs with smooth activation functions, the training dynamics in MLPs with non-smooth activations are noticeably less prominent. In this section, we provide some brief intuition for why this is the case. In particular, recall a step in our proof sketch of Theorem 3.5: when we assume ϕ is smooth, then $\sigma_i(G_1(0)) = \Theta(\epsilon)$ for all $i \geq K + 1$. Our next result shows that in a simplified setting, this step does not hold for a nonsmooth ϕ . Specifically, we show (most of) these tail singular values of $G_1(0)$ are *not* on the same order as ϵ . Although the theoretical setting is highly simplified, we empirically observe similar conclusions hold in broader settings; see Section B.1. The proof of Proposition B.1 is provided in Appendix E.

Proposition B.1. *Suppose $d = N$, $W_1(0)_{ij} \stackrel{iid}{\sim} \mathcal{N}(0, \frac{\epsilon^2}{m})$, and $\phi = \text{ReLU}$. Then, for any $\delta \in (0, 1)$, with probability at least $1 - \delta$ w.r.t. the randomness in $W_1(0)$,*

$$\sigma_{d-K}(G_1(0)) \geq \sqrt{\frac{\lambda_{\min}(V^\top DV)}{4} - \left(\frac{R'}{6} \cdot \log\left(\frac{2(d-K)}{\delta}\right) + \sqrt{2 \cdot \log\left(\frac{2(d-K)}{\delta}\right) \cdot \frac{R' \cdot \lambda_{\max}(V^\top DV)}{16}} \right)},$$

where $V \in \mathbb{R}^{d \times (d-K)}$ is an orthonormal basis for $\mathcal{N}(W_2^\top \Delta_2(0))$, $D := \text{diag}\left(\left\| (W_2^\top \Delta_2(0))_{:,1} \right\|_2^2, \dots, \left\| (W_2^\top \Delta_2(0))_{:,N} \right\|_2^2\right)$, and $R' := \max_{i \in [m]} \left\| (W_2^\top \Delta_2(0))_{i,:} \right\|_2^2$.

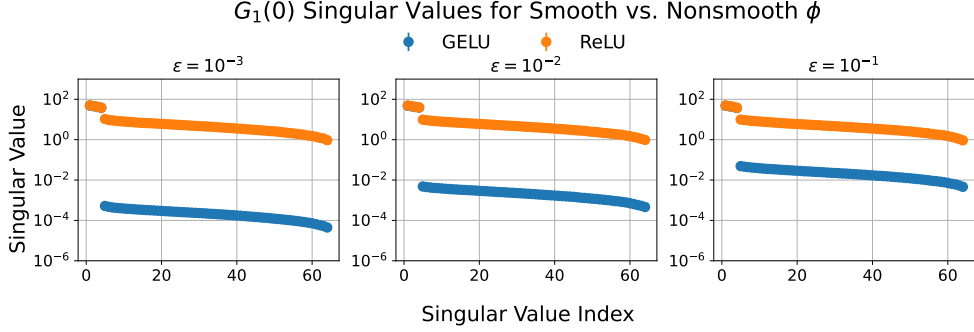


Figure 11: The bottom $d - K$ singular values of $G_1(0)$ scale with ϵ when ϕ is smooth (GELU), but do not change with ϵ when ϕ is nonsmooth (ReLU). The top- K singular values of $G_1(0)$ overlap for both smooth and nonsmooth ϕ .

Intuition behind Proposition B.1. Below, we provide some intuition behind Proposition B.1. First, note for small ϵ , we have $\Delta_2(0) \approx -Y$, and so $W_2^\top \Delta_2(0) \approx -W_2^\top Y \in \mathbb{R}^{m \times N}$. If we consider a classification task with balanced classes and one-hot encoded labels, we have $Y = I_K \otimes \mathbf{1}_n^\top$, where $n = N/K$. Thus,

$$W_2^\top Y = \begin{bmatrix} (W_2)_{1,1} \mathbf{1}_n^\top & \dots & (W_2)_{K,1} \mathbf{1}_n^\top \\ \vdots & \ddots & \vdots \\ (W_2)_{1,m} \mathbf{1}_n^\top & \dots & (W_2)_{K,m} \mathbf{1}_n^\top \end{bmatrix},$$

i.e., the columns of $W_2^\top Y$ are (repeated) rows of W_2 which are of size m , and each row of $W_2^\top Y$ contains $n = N/K = d/K$ copies of the corresponding column entries of W_2 , which are each of size K . Next, if W_2 contains, e.g., iid sub-Gaussian entries with zero mean and unit variance, then $\left\| - (W_2^\top Y)_{i,:} \right\|_2^2 \approx d$ and $\left\| - (W_2^\top Y)_{:,j} \right\|_2^2 \approx m$, and so $D \approx mI_N \implies V^\top DV \approx mI_{d-K} \implies \lambda_{\min}(V^\top DV) \approx \lambda_{\max}(V^\top DV) \approx m$, and $R' \approx d$. For a fixed failure probability $\delta \in (0, 1)$, we have

$$\sigma_{d-K}(G_1(0)) \gtrsim \sqrt{\Theta(m) - \Theta(d \log d) - \Theta(\sqrt{md \log d})}.$$

Then, if $m \gtrsim \Omega(d \log d)$, this lower bound is non-vacuous and not of the same order as the initialization scale ϵ .

New assumptions on X and $W_1(0)$. In Proposition B.1, we assume $d = N$, i.e., X is an exactly orthogonal matrix, and $(W_1(0))_{ij} \sim \mathcal{N}\left(0, \frac{\epsilon^2}{m}\right)$. This is mostly for ease of analysis, specifically to introduce iid random variables in the mask $\phi'(W_1(0)X)$. Although we recognize $d = N$ is quite restrictive, we empirically show the broader conclusions hold in more general settings, i.e., $d < N$. Next, since independent Gaussian vectors are approximately orthogonal in high dimensions, $W_1(0)$ in Proposition B.1 satisfies $W_1^\top(0)W_1(0) \approx \epsilon^2 I_d$, which is the assumption we make on $W_1(0)$ in Theorem 3.5.

B.1 Verifying Proposition B.1

Here, we provide empirical evidence supporting Proposition B.1. In particular, we show that when $\phi = \text{ReLU}$, the tail singular values of $G_1(0)$ are independent of the (small) initialization scale ϵ . Here, all experiments were done in `numpy` on a Macbook Air with an M3 chip. We adhered to the same data generation process and network initialization schemes as in Figure 3, but with $\epsilon \in \{10^{-3}, 10^{-2}, 10^{-1}\}$. We note this setting violates the assumptions on X and $W_1(0)$ in Proposition B.1. We computed the singular values of $G_1(0)$ for both $\phi = \text{GELU}$ and $\phi = \text{ReLU}$ over 10 trials.

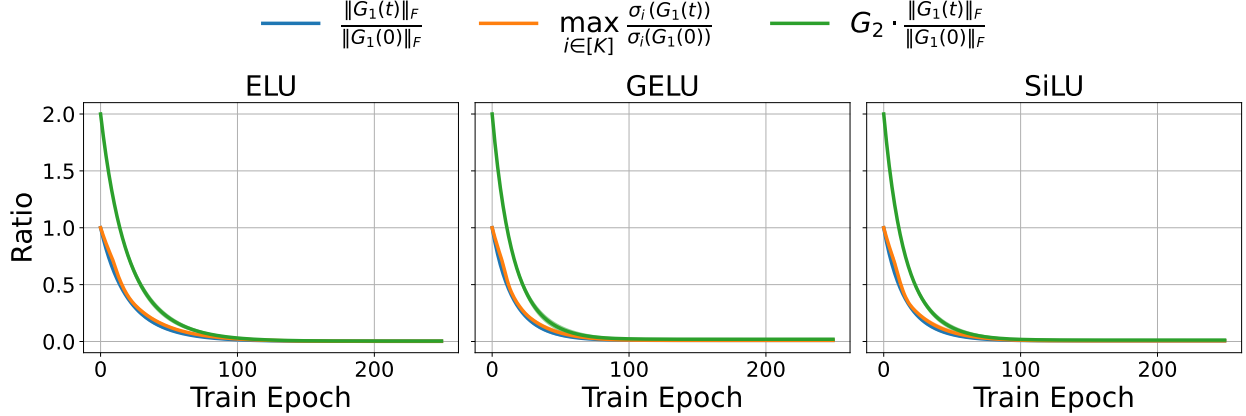


Figure 12: The gradient norm and top- K singular values appear to monotonically decay from their initial values, despite the objective being non-convex.

Results. All d singular values of $G_1(0)$ are shown in Figure 11. Clearly, when $\phi = \text{GELU}$, the tail singular values of $G_1(0)$ scale linearly with ϵ . Meanwhile, when $\phi = \text{ReLU}$, the bottom $d - K$ singular values appear to be on a similar order as the top- K and *independent* of ϵ . This supports our broader conclusions from Proposition B.1, despite the specific theoretical assumptions in Proposition B.1 being violated here.

C Empirical Justifications for Assumption 3.4

In this section, we provide some empirical justification for Assumption 3.4, particularly regarding the gradient norm and singular values. We adopt the exact same data generation process, network architecture, and training method as in Figure 3, but train for 250 epochs instead of 100.

Gradient norm and singular value decay. In Figure 12, we show $\|G_1(t)\|_F$ decays monotonically with respect to $\|G_1(0)\|_F$, and that the top- K singular values of $G_1(t)$ decay at a similar rate. Specifically, we plot $\frac{\|G_1(t)\|_F}{\|G_1(0)\|_F}$, $\max_{i \in [K]} \frac{\sigma_i(G_1(t))}{\sigma_i(G_1(0))}$, and $G_2 \cdot \frac{\|G_1(t)\|_F}{\|G_1(0)\|_F}$, where $G_2 = 2$. The gradient norm clearly monotonically decays throughout training, despite the objective being non-convex. This supports the assumption that $\|G_1(t)\|_F \leq G_1 \cdot (1 - \Theta(\eta))^{\Theta(t)} \cdot \|G_1(0)\|_F$. Additionally, all of the top- K singular values of $G_1(t)$ appear to decay at a similar rate, as Figure 12 shows $\frac{\sigma_i(G_1(t))}{\sigma_i(G_1(0))} \leq G_2 \cdot \frac{\|G_1(t)\|_F}{\|G_1(0)\|_F}$ for $i \in [K]$, which supports that assumption as well.

Finally, we show the tail singular values of $G_1(t)$ remain much smaller than $\sigma_K(W_2^\top Y X^\top)$. Figure 13 plots $\sigma_K(W_2^\top Y X^\top)$ vs. $\sigma_{K+1}(G_1(t))$ for different ϵ , all averaged over 10 trials. Clearly, $\sigma_K(W_2^\top Y X^\top)$ is much larger than $\sigma_{K+1}(G_1(t))$, justifying our assumption that $\sigma_K(W_2^\top Y X^\top) - \sigma_{K+1}(G_1(t)) \geq G_3 \cdot \sigma_K(W_2^\top Y X^\top)$. For all 3 activations, $\sigma_{K+1}(G_1(t))$ remains very small for all GD iterations. We conjecture this is because under our setting, the network is approximately linear, i.e., $W_2 \phi(W_1(t)X) \approx \phi'(0) \cdot W_2 W_1(t)X$, and so $G_1(t) \approx \left(\nabla_{W_1} \frac{1}{2} \cdot \|\phi'(0) \cdot W_2 W_1(t)X - Y\|_F^2 \right) + E$ for some “small” perturbation E .

D Proofs for Theorem 3.5

In this section, we first re-state our assumptions in Appendix D.1, and derive the analytical form of the loss gradient with respect to (w.r.t.) W_1 in Appendix D.2. We then provide supporting lemmas for Theorem 3.5 with their proofs in Appendix D.3, and the proof of Theorem 3.5 in Section D.4.

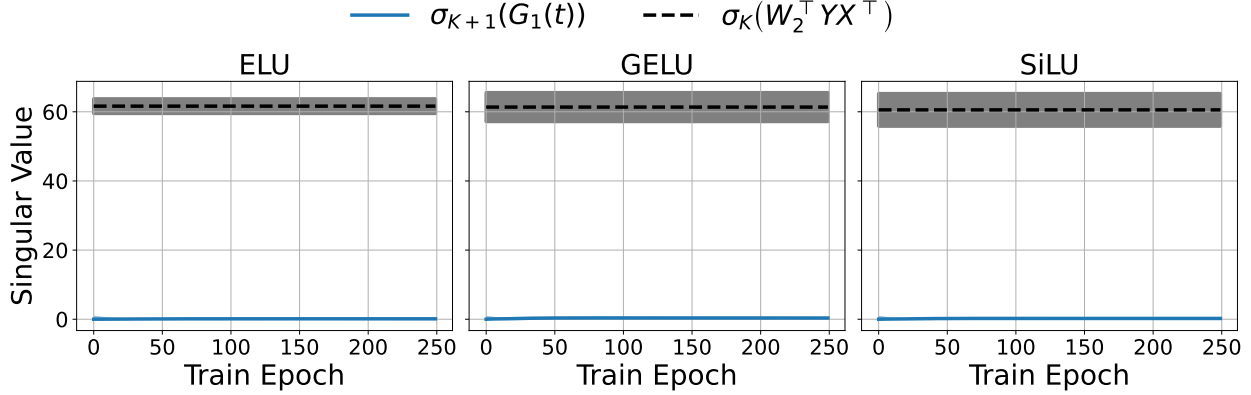


Figure 13: Throughout training, $\sigma_{K+1}(G_1(t))$ remains significantly smaller than $\sigma_K(W_2^T Y X^T)$.

D.1 Notation and Assumptions

Here, we re-state our notation and assumptions for Theorem 3.5 for convenience, and introduce some new notation.

Notation. We use unbolted letters x, X for scalars, bold lower case letters x for vectors, and bold capital letters X for matrices. For some $N \in \mathbb{N}$, $[N]$ denotes the set $\{1, 2, \dots, N\}$. For scalars a, b , we say $a \lesssim O(b)$ if there exists a constant C s.t. $a \leq C \cdot b$, $a \gtrsim \Omega(b)$ if $a \geq C \cdot b$, and $a = \Theta(b)$ if $a = C \cdot b$. We use $\sigma_i(X)$, $\|X\|_F$, $\|X\|_1$, $\|X\|_\infty$, and $\|X\|_{\max}$ to respectively denote the i^{th} singular value, Frobenius norm, matrix-1 norm, matrix- ∞ norm, and maximum magnitude element, and use $X_{i,:}$ and $X_{:,j}$ to respectively denote the i^{th} row and j^{th} column of X , where $X_{i,:}$ is written as a column vector. Finally, $\mathcal{R}(X)$ denotes the range (or column space) of X , and $\mathcal{R}^\perp(X)$ its orthogonal complement.

We now re-state our assumptions here for convenience.

Assumption 3.2 (Input data). The data $X \in \mathbb{R}^{d \times N}$ is whitened, and the label dimension K satisfies $K < d/2$.

Assumption 3.3 (Network architecture and training). The network (1) contains $L = 2$ layers, i.e., $f_\Theta(X) =: f_{W_1}(X) = W_2 \phi(W_1 X)$, with $W_1 \in \mathbb{R}^{m \times d}$ and $W_2 \in \mathbb{R}^{K \times m}$. Furthermore,

- The width m satisfies $m \geq d$,
- The activation function ϕ satisfies $\phi(0) = 0$, $|\phi'(x)| \leq \beta$, and $|\phi''(x)| \leq \mu$ for all $x \in \mathbb{R}$.
- The network is trained using GD with step size η on the squared error loss:

$$\min_{W_1} \mathcal{L}(W_1) = \frac{1}{2} \|f_{W_1}(X) - Y\|_F^2, \quad (4)$$

where W_2 is fixed during training and is full row rank.

Again, here we sometimes use $f_{W_1}(X)$ to denote $f_\Theta(X)$. Finally, we make some additional technical assumptions to make the result more interpretable, which we re-state below.

Assumption 3.4. Define $\Delta_2(t) = W_2 \phi(W_1(t)X) - Y$ and $G_1(t) = \nabla_{W_1} \mathcal{L}(W_1(t))$. For all $t \geq 0$,

- $\|\Delta_2(t)\|_{\max} \leq M$ for some finite constant M , and
- there exist constants G_1, G_2 , and G_3 such that $G_1(t)$ satisfies the following:

$$\frac{\|G_1(t)\|_F}{\|G_1(0)\|_F} \leq G_1 \cdot (1 - \Theta(\eta))^{\Theta(t)},$$

$$\frac{\sigma_i(G_1(t))}{\sigma_i(G_1(0))} \leq G_2 \cdot \frac{\|G_1(t)\|_F}{\|G_1(0)\|_F}, \quad \text{for all } i \leq K, \text{ and}$$

$$\sigma_K(W_2^\top Y X^\top) - \sigma_{K+1}(G_1(t)) \geq G_3 \cdot \sigma_K(W_2^\top Y X^\top)$$

D.2 Analytical Gradient Form

Here, we derive the analytical form of the loss gradient w.r.t. W_1 , which we denote as G_1 . Recall

$$H_0 = X \in \mathbb{R}^{d \times N}, \quad Z_1 = W_1 H_0 \in \mathbb{R}^{m \times N}, \quad H_1 = \phi(Z_1) \in \mathbb{R}^{m \times N}, \quad \text{and} \quad Z_2 = W_2 H_1 \in \mathbb{R}^{K \times N}.$$

Notice $Z_2 = f_{W_1}(X)$. Define

$$\Delta_2 = \nabla_{Z_2} \mathcal{L}(W_1) = Z_2 - Y \in \mathbb{R}^{K \times N} \quad \text{and}$$

$$\Delta_1 = \nabla_{Z_1} \mathcal{L}(W_1) = (\nabla_{Z_1} H_1)^\top (\nabla_{H_1} Z_2)^\top \nabla_{Z_2} \mathcal{L}(W_1) = W_2^\top \Delta_2 \odot \phi'(Z_1) \in \mathbb{R}^{m \times N},$$

where $\phi'(\cdot)$ is the derivative of activation function $\phi(\cdot)$. The gradient of the loss w.r.t. W_1 via backpropagation is

$$G_1 := \nabla_{W_1} \mathcal{L}(W_1) = \Delta_1 H_0^\top = \Delta_1 X^\top. \quad (11)$$

For all $t > 0$ and $l \in \{1, 2\}$, let $Z_l(t)$, $H_l(t)$, $\Delta_l(t)$, and $G_l(t)$ denote the values of their corresponding matrices at iteration t . Then,

$$\Delta_2(t) = Z_2(t) - Y, \quad \Delta_1(t) = W_2^\top(t) \Delta_2(t) \odot \phi'(Z_1(t)), \quad \text{and} \quad G_1(t) = \Delta_1(t) X^\top.$$

Substituting the expression for $\Delta_1(t)$ into $G_1(t)$ yields

$$G_1(t) = \Delta_1(t) H_0^\top = \left(W_2^\top \Delta_2(t) \odot \phi'(Z_1(t)) \right) X^\top = \left(W_2^\top (Z_2(t) - Y) \odot \phi'(W_1(t) X) \right) X^\top. \quad (12)$$

D.3 Supporting Results

In this section, we provide supporting results that are useful in proving Theorem 3.5. For notational brevity, we use $\ell(t) := \mathcal{L}(W_1(t)) = \ell(Z_2(t), Y)$ to denote the value of the loss at GD iteration t .

D.3.1 Auxiliary Results

In this section, we provide auxiliary results in linear algebra. First, for a matrix A , we define $|A|$ as applying $|\cdot|$ element-wise to A , i.e., $|A|_{ij} = |A_{ij}|$. Our first result relates the spectral norm of A with $|A|$.

Lemma D.1. *For any $A \in \mathbb{R}^{m \times n}$, we have $\sigma_1(A) \leq \sigma_1(|A|)$.*

Proof. For some square matrix $B \in \mathbb{R}^{n \times n}$, let $\rho(B)$ denote its spectral radius. Without loss of generality, suppose $m \geq n$. By definition, we have $\sigma_1^2(A) = \rho(A^\top A)$, so we focus on upper bounding $\rho(A^\top A)$ in terms of $\rho(|A^\top A|)$. First, we trivially have $A^\top A \leq |A^\top A|$, where \leq is done element-wise. From [Horn and Johnson \(2012, Exercise 8.1.9\)](#),

$$|A^\top A| \leq |A|^\top |A|.$$

Then, applying [Horn and Johnson \(2012, Theorem 8.1.18\)](#) twice yields

$$\rho(A^\top A) \leq \rho(|A^\top A|) \leq \rho(|A|^\top |A|),$$

which implies

$$\sigma_1^2(A) = \rho(A^\top A) \leq \rho(|A|^\top |A|) = \sigma_1^2(|A|),$$

which completes the proof. \square

Our next result applies upper bounds on the matrix ∞ and 1 norms on products of particular matrix types.

Lemma D.2. Suppose $\mathbf{W} \in \mathbb{R}^{m \times d}$ satisfies $\mathbf{W}^\top \mathbf{W} = \epsilon^2 \mathbf{I}_d$, and $\mathbf{X} \in \mathbb{R}^{d \times N}$ satisfies $\mathbf{X} \mathbf{X}^\top = \mathbf{I}_d$. Then, we have

$$\|\mathbf{W}\mathbf{X} \odot \mathbf{W}\mathbf{X}\|_\infty \leq \epsilon^2 \quad \text{and} \quad \|\mathbf{W}\mathbf{X} \odot \mathbf{W}\mathbf{X}\|_1 \leq \epsilon^2.$$

Proof. Define $\mathbf{Z} := \mathbf{W}\mathbf{X}$. Notice $(\mathbf{Z} \odot \mathbf{Z})_{ij} = \mathbf{Z}_{ij}^2$, and so $\|\mathbf{Z} \odot \mathbf{Z}\|_\infty$ and $\|\mathbf{Z} \odot \mathbf{Z}\|_1$ are the maximum row and column squared Euclidean norms of \mathbf{Z} . Next, notice the i^{th} row of \mathbf{Z} is $\mathbf{Z}_{i,:} := \mathbf{W}_{i,:}^\top \mathbf{X}$. Therefore,

$$\|\mathbf{Z}_{i,:}\|_2^2 = \|\mathbf{W}_{i,:}^\top \mathbf{X}\|_2^2 = \mathbf{W}_{i,:}^\top \mathbf{X} \mathbf{X}^\top \mathbf{W}_{i,:} = \mathbf{W}_{i,:}^\top \mathbf{W}_{i,:} = \|\mathbf{W}_{i,:}\|_2^2.$$

Since \mathbf{W} has ϵ -scaled orthonormal columns, we have $\|\mathbf{W}_{i,:}\|_2^2 \leq \epsilon^2$ for all $i \in [m]$. Therefore,

$$\|\mathbf{Z} \odot \mathbf{Z}\|_\infty = \max_{i \in [m]} \|\mathbf{Z}_{i,:}\|_2^2 = \max_{i \in [m]} \|\mathbf{W}_{i,:}^\top \mathbf{X}\|_2^2 = \max_{i \in [m]} \|\mathbf{W}_{i,:}\|_2^2 \leq \epsilon^2.$$

Similarly, the j^{th} column of \mathbf{Z} is $\mathbf{Z}_{:,j} = \mathbf{W}\mathbf{X}_{:,j}$. Therefore,

$$\|\mathbf{Z}_{:,j}\|_2^2 = \|\mathbf{W}\mathbf{X}_{:,j}\|_2^2 = \mathbf{X}_{:,j}^\top \mathbf{W}^\top \mathbf{W}\mathbf{X}_{:,j} = \epsilon^2 \mathbf{X}_{:,j}^\top \mathbf{X}_{:,j} = \epsilon^2 \|\mathbf{X}_{:,j}\|_2^2.$$

Since \mathbf{X} is whitened, i.e., $\mathbf{X} \mathbf{X}^\top = \mathbf{I}_d$, we have $\|\mathbf{X}_{:,j}\|_2^2 \leq 1$ for all $j \in [N]$. Therefore,

$$\|\mathbf{Z} \odot \mathbf{Z}\|_1 = \max_{j \in [N]} \|\mathbf{Z}_{:,j}\|_2^2 = \max_{j \in [N]} \|\mathbf{W}\mathbf{X}_{:,j}\|_2^2 = \max_{j \in [N]} \epsilon^2 \|\mathbf{X}_{:,j}\|_2^2 \leq \epsilon^2.$$

This completes the proof. \square

Next, for two matrices $\mathbf{U}_1 \in \mathbb{R}^{d \times r}$, $\mathbf{U}_2 \in \mathbb{R}^{d \times r}$ with orthonormal columns, recall the definition of $\|\sin \Theta(\mathbf{U}_1, \mathbf{U}_2)\|_2$ in Definition 3.1. Also define

$$\text{dist}(\mathbf{U}_1, \mathbf{U}_2) = \|\mathbf{U}_1 \mathbf{U}_1^\top - \mathbf{U}_2 \mathbf{U}_2^\top\|_F. \quad (13)$$

The next result relates $\|\sin \Theta(\mathbf{U}_1, \mathbf{U}_2)\|_2$ and $\text{dist}(\mathbf{U}_1, \mathbf{U}_2)$.

Lemma D.3. Let $\mathbf{U}_1, \mathbf{U}_2 \in \mathbb{R}^{d \times K}$ have orthonormal columns, and $\mathbf{U}_{1,\perp} \in \mathbb{R}^{d \times (d-K)}$ have orthonormal columns that satisfy $\mathbf{U}_1^\top \mathbf{U}_{1,\perp} = \mathbf{0}_{K \times (d-K)}$. Then,

$$\text{dist}(\mathbf{U}_1, \mathbf{U}_2) = \sqrt{2} \cdot \|\sin \Theta(\mathbf{U}_1, \mathbf{U}_2)\|_2 = \sqrt{2} \cdot \|\mathbf{U}_{1,\perp}^\top \mathbf{U}_2\|_F.$$

Proof. Let $\theta_1, \dots, \theta_K$ denote the K principal angles between \mathbf{U}_1 and \mathbf{U}_2 , which are exactly $\theta_i = \arccos(\sigma_i(\mathbf{U}_1^\top \mathbf{U}_2))$. Then, from Xu et al. (2025, Lemma 2), we have

$$\text{dist}(\mathbf{U}_1, \mathbf{U}_2) = \sqrt{2} \cdot \sqrt{\sum_{i=1}^K \sin^2(\theta_i)} = \sqrt{2} \cdot \|\sin \Theta(\mathbf{U}_1, \mathbf{U}_2)\|_2.$$

It suffices to show that $\|\sin \Theta(\mathbf{U}_1, \mathbf{U}_2)\|_2 = \|\mathbf{U}_{1,\perp}^\top \mathbf{U}_2\|_F$. We can write

$$\mathbf{U}_2 = \mathbf{U}_1 \mathbf{U}_1^\top \mathbf{U}_2 + \mathbf{U}_{1,\perp} \mathbf{U}_{1,\perp}^\top \mathbf{U}_2.$$

Therefore,

$$\begin{aligned} \|\mathbf{U}_{1,\perp}^\top \mathbf{U}_2\|_F^2 &= \|\mathbf{U}_2\|_F^2 - \|\mathbf{U}_1^\top \mathbf{U}_2\|_F^2 = K - \sum_{i=1}^K \sigma_i^2(\mathbf{U}_1^\top \mathbf{U}_2) \\ &= K - \sum_{i=1}^K \cos^2(\theta_i) = \sum_{i=1}^K (1 - \cos^2(\theta_i)) = \sum_{i=1}^K \sin^2(\theta_i) = \|\sin \Theta(\mathbf{U}_1, \mathbf{U}_2)\|_2^2. \end{aligned}$$

This completes the proof. \square

Our next result upper bounds the alignment between two subspaces after being projected onto a third subspace.

Lemma D.4. *Let $Q \in \mathbb{R}^{m \times d}$ and $U_1, U_2 \in \mathbb{R}^{m \times K}$ all have orthonormal columns. Define $U_{1,\perp} \in \mathbb{R}^{m \times (m-K)}$ to have orthonormal columns that satisfy $U_1^\top U_{1,\perp} = \mathbf{0}_{K \times (m-K)}$, and $\tilde{U}_{1,\perp} \in \mathbb{R}^{d \times (d-K)}$ to be an orthonormal basis for the subspace $\mathcal{R}^\perp(Q^\top U_1)$. Then, we have*

$$\|U_2^\top Q \tilde{U}_{1,\perp}\|_F \leq \|U_2^\top U_{1,\perp}\|_F.$$

Proof. Since $U_1 \in \mathbb{R}^{m \times K}$ and $U_2 \in \mathbb{R}^{m \times (m-K)}$ each have orthonormal columns, and $U_1^\top U_{1,\perp} = \mathbf{0}_{m \times (m-K)}$, we have

$$I_m = U_1 U_1^\top + U_{1,\perp} U_{1,\perp}^\top.$$

Therefore,

$$\begin{aligned} U_2^\top Q \tilde{U}_{1,\perp} &= U_2^\top (U_1 U_1^\top + U_{1,\perp} U_{1,\perp}^\top) Q \tilde{U}_{1,\perp} \\ &= \underbrace{U_2^\top U_1 U_1^\top Q \tilde{U}_{1,\perp}}_{(a)} + U_2^\top U_{1,\perp} U_{1,\perp}^\top Q \tilde{U}_{1,\perp}. \end{aligned}$$

Since $\tilde{U}_{1,\perp} \in \mathcal{R}^\perp(Q^\top U_1)$, we have $U_1^\top Q \tilde{U}_{1,\perp} = (Q^\top U_1)^\top \tilde{U}_{1,\perp} = \mathbf{0}_{K \times (d-K)}$, and so $(a) = \mathbf{0}_{K \times (d-K)}$. Thus,

$$\begin{aligned} \|U_2^\top Q \tilde{U}_{1,\perp}\|_F &= \|U_2^\top U_{1,\perp} U_{1,\perp}^\top Q \tilde{U}_{1,\perp}\|_F \\ &\leq \|U_2^\top U_{1,\perp}\|_F \cdot \sigma_1(U_{1,\perp}^\top Q \tilde{U}_{1,\perp}) \leq \|U_2^\top U_{1,\perp}\|_F \cdot \sigma_1(U_{1,\perp}) \cdot \sigma_1(Q) \cdot \sigma_1(\tilde{U}_{1,\perp}) = \|U_2^\top U_{1,\perp}\|_F. \end{aligned}$$

This completes the proof. □

Our last auxiliary is a version of Wedin's Sin Theorem from [Wedin \(1972\)](#).

Lemma D.5. *Let $\tilde{A} = A + P \in \mathbb{R}^{m \times d}$ ($m \geq d$) for some matrices A and P , where*

$$A := [L_1(A) \quad L_2(A)] \begin{bmatrix} \sigma_1(A) & & \\ & \ddots & \\ 0 & \dots & \sigma_d(A) \end{bmatrix} \begin{bmatrix} R_1^\top(A) \\ R_2^\top(A) \end{bmatrix},$$

and

$$\tilde{A} := [L_1(\tilde{A}) \quad L_2(\tilde{A})] \begin{bmatrix} \sigma_1(\tilde{A}) & & \\ & \ddots & \\ 0 & \dots & \sigma_d(\tilde{A}) \end{bmatrix} \begin{bmatrix} R_1^\top(\tilde{A}) \\ R_2^\top(\tilde{A}) \end{bmatrix}$$

respectively denote SVDs of A and \tilde{A} , with $L_1(A)$ ($R_1(A)$) denoting the top- K left (right) singular subspaces of A , and $L_2(A)$ ($R_2(A)$) denoting the bottom $m - K$ ($d - K$) left (right) singular subspaces of A . Then, we have

$$\max \left\{ \left\| \sin \Theta(L_1(\tilde{A}), L_1(A)) \right\|_2, \left\| \sin \Theta(R_1(\tilde{A}), R_1(A)) \right\|_2 \right\} \leq \frac{\|P\|_F}{\sigma_K(\tilde{A}) - \sigma_{K+1}(A)}.$$

Proof. First, from the Generalized Sin Θ Theorem in [Wedin \(1972\)](#), we have

$$\max \left\{ \left\| \sin \Theta(L_1(\tilde{A}), L_1(A)) \right\|_2, \left\| \sin \Theta(R_1(\tilde{A}), R_1(A)) \right\|_2 \right\} \leq \frac{\max \left\{ \|P^\top L_1(\tilde{A})\|_F, \|P R_1(\tilde{A})\|_F \right\}}{\sigma_K(\tilde{A}) - \sigma_{K+1}(A)}.$$

Next, since $L_1(\tilde{A})$ has orthonormal columns, we have

$$\left\| P^\top L_1(\tilde{A}) \right\|_F \leq \|P\|_F \cdot \sigma_1(L_1(\tilde{A})) = \|P\|_F.$$

We can use identical steps to show $\left\| PR_1(\tilde{A}) \right\|_F \leq \|P\|_F$. This completes the proof. \square

D.3.2 Gradient Bounds

In this section, we provide bounds related to the gradient $G_1(t)$. First, we upper bound $\|G_1(t)\|_F$.

Lemma D.6. *For all $t \geq 0$, we have*

$$\|G_1(t)\|_F \leq \beta \cdot \sigma_1(W_2) \cdot \sqrt{2\ell(t)}.$$

Proof. Recall from Equation (12), we have

$$G_1(t) = \left(W_2^\top \Delta_2(t) \odot \phi'(\mathbf{Z}_1(t)) \right) \mathbf{X}^\top,$$

and so

$$\begin{aligned} \|G_1(t)\|_F &= \left\| \left(W_2^\top \Delta_2(t) \odot \phi'(\mathbf{Z}_1(t)) \right) \mathbf{X}^\top \right\|_F \leq \|W_2^\top \Delta_2(t) \odot \phi'(\mathbf{Z}_1(t))\|_F \cdot \sigma_1(\mathbf{X}) \\ &\stackrel{(i)}{=} \|W_2^\top \Delta_2(t) \odot \phi'(\mathbf{Z}_1(t))\|_F \stackrel{(ii)}{\leq} \beta \cdot \|W_2^\top \Delta_2(t)\|_F = \beta \cdot \sigma_1(W_2) \cdot \|\Delta_2(t)\|_F, \end{aligned}$$

where (i) is because $\mathbf{X}\mathbf{X}^\top = \mathbf{I}_d$, and (ii) is because ϕ is β -Lipschitz. Finally, note

$$\ell(t) = \frac{1}{2} \|W_2 \phi(W_2(t) \mathbf{X}) - \mathbf{Y}\|_F^2 = \frac{1}{2} \|\Delta_2(t)\|_F^2 \implies \|\Delta_2(t)\|_F = \sqrt{2\ell(t)}.$$

Putting everything together yields

$$\|G_1(t)\|_F \leq \beta \cdot \sigma_1(W_2) \cdot \sqrt{2\ell(t)},$$

which completes the proof. \square

Next, we show the gradient $G_1(t)$ is locally Lipschitz.

Lemma D.7. *Suppose $W_1(0) \in \mathbb{R}^{m \times d}$ is an arbitrary ϵ -scaled semi-orthogonal matrix, i.e., $W_1^\top(0)W_1(0) = \epsilon^2 \mathbf{I}_d$. Define $\Delta_2(W_1) := W_2 \phi(W_1 \mathbf{X}) - \mathbf{Y}$, and $\mathcal{M} := \{W_1 \in \mathbb{R}^{m \times d} : \|\Delta_2(W_1)\|_{\max} \leq M\}$. Also define $G_1(W_1)$ to be G_1 at some $W_1 \in \mathbb{R}^{m \times d}$. Then, for all $W_1, \tilde{W}_1 \in \mathcal{M}$, we have*

$$\|G_1(W_1) - G_1(\tilde{W}_1)\|_F \leq (\mu \cdot M \cdot \|W_2\|_1 + \beta^2 \cdot \sigma_1^2(W_2)) \cdot \|W_1 - \tilde{W}_1\|_F.$$

Proof. Suppose $W_1, \tilde{W}_1 \in \mathcal{M}$. Let $G_1(W_1), G_1(\tilde{W}_1)$ denote G_1 at W_1 and \tilde{W}_1 , and let $\Delta_2 := \Delta_2(W_1)$ and $\tilde{\Delta}_2 := \Delta_2(\tilde{W}_1)$. Then, we have

$$\begin{aligned} &\left\| G_1(W_1) - G_1(\tilde{W}_1) \right\|_F \\ &= \left\| \left(W_2^\top \Delta_2 \odot \phi'(\mathbf{W}_1 \mathbf{X}) - W_2^\top \tilde{\Delta}_2 \odot \phi'(\tilde{W}_1 \mathbf{X}) \right) \mathbf{X}^\top \right\|_F \\ &\leq \left\| W_2^\top \Delta_2 \odot \phi'(\mathbf{W}_1 \mathbf{X}) - W_2^\top \Delta_2 \odot \phi'(\tilde{W}_1 \mathbf{X}) \right\|_F \\ &= \left\| W_2^\top \Delta_2 \odot \phi'(\mathbf{W}_1 \mathbf{X}) - W_2^\top \Delta_2 \odot \phi'(\tilde{W}_1 \mathbf{X}) + W_2^\top \Delta_2 \odot \phi'(\tilde{W}_1 \mathbf{X}) - W_2^\top \Delta_2 \odot \phi'(\tilde{W}_1 \mathbf{X}) \right\|_F \end{aligned}$$

$$\begin{aligned}
&\leq \left(\left\| \mathbf{W}_2^\top \Delta_2 \odot \left(\phi'(\mathbf{W}_1 \mathbf{X}) - \phi'(\widehat{\mathbf{W}}_1 \mathbf{X}) \right) \right\|_F + \left\| \mathbf{W}_2^\top (\Delta_2 - \widehat{\Delta}_2) \odot \phi'(\widehat{\mathbf{W}}_1 \mathbf{X}) \right\|_F \right) \\
&= \left(\left\| \mathbf{W}_2^\top \Delta_2 \odot \left(\phi'(\mathbf{W}_1 \mathbf{X}) - \phi'(\widehat{\mathbf{W}}_1 \mathbf{X}) \right) \right\|_F + \left\| \mathbf{W}_2^\top \mathbf{W}_2 \left(\phi(\mathbf{W}_1 \mathbf{X}) - \phi(\widehat{\mathbf{W}}_1 \mathbf{X}) \right) \odot \phi'(\widehat{\mathbf{W}}_1 \mathbf{X}) \right\|_F \right) \\
&\leq \left(\left\| \mathbf{W}_2^\top \Delta_2 \right\|_{\max} \cdot \left\| \phi'(\mathbf{W}_1 \mathbf{X}) - \phi'(\widehat{\mathbf{W}}_1 \mathbf{X}) \right\|_F + \beta \cdot \sigma_1^2(\mathbf{W}_2) \cdot \left\| \phi(\mathbf{W}_1 \mathbf{X}) - \phi(\widehat{\mathbf{W}}_1 \mathbf{X}) \right\|_F \right) \\
&\stackrel{(i)}{\leq} \left(\mu \cdot \left\| \mathbf{W}_2 \right\|_1 \cdot \left\| \Delta_2 \right\|_{\max} \cdot \left\| \mathbf{W}_1 \mathbf{X} - \widehat{\mathbf{W}}_1 \mathbf{X} \right\|_F + \beta^2 \cdot \sigma_1^2(\mathbf{W}_2) \cdot \left\| \mathbf{W}_1 \mathbf{X} - \widehat{\mathbf{W}}_1 \mathbf{X} \right\|_F \right) \\
&\stackrel{(ii)}{\leq} (\mu \cdot M \cdot \left\| \mathbf{W}_2 \right\|_1 + \beta^2 \cdot \sigma_1^2(\mathbf{W}_2)) \cdot \left\| \mathbf{W}_1 - \widehat{\mathbf{W}}_1 \right\|_F,
\end{aligned}$$

where (i) is because ϕ and β -Lipschitz and μ -smooth, and (ii) is because $\mathbf{W}_1, \widehat{\mathbf{W}}_1 \in \mathcal{M}$, which implies $\left\| \Delta_2 \right\|_{\max} \leq M$ by definition. This completes the proof. \square

From now on, we define $\gamma_L := \mu \cdot M \cdot \left\| \mathbf{W}_2 \right\|_1 + \beta^2 \cdot \sigma_1^2(\mathbf{W}_2)$. Note that by the Descent Lemma (Bertsekas, 1997), if $\eta \leq \frac{1}{\gamma_L}$, then the loss does not increase. Thus, we assume $\eta \leq \frac{1}{\gamma_L}$.

D.3.3 Gradient Singular Values and Subspaces

In this section, we provide results characterizing the singular values and subspaces of the gradient. Before proceeding, we provide some additional definitions. Let $\mathbf{G}_1(t) = \mathbf{L}_1(t) \Sigma_1(t) \mathbf{R}_1^\top(t)$ denote an SVD of $\mathbf{G}_1(t)$, with $\mathbf{L}_{1,1}(t) \in \mathbb{R}^{m \times K}$, $\Sigma_{1,1}(t) \in \mathbb{R}^{K \times K}$, and $\mathbf{R}_{1,1}(t) \in \mathbb{R}^{d \times K}$ denoting the top- K components, and $\mathbf{L}_{1,2}(t) \in \mathbb{R}^{m \times (d-K)}$, $\Sigma_{1,2}(t) \in \mathbb{R}^{(d-K) \times (d-K)}$, and $\mathbf{R}_{1,2}(t) \in \mathbb{R}^{d \times (d-K)}$ denoting the bottom $d - K$ components.

Our first result shows under small initialization scale ϵ , $\mathbf{G}_1(0)$ is approximately rank- K .

Lemma D.8. *Suppose Assumptions 3.2 and 3.3 hold. Define*

$$r(\epsilon) = \epsilon \cdot \phi'(0) \cdot \sigma_1^2(\mathbf{W}_2) \cdot \left(\phi'(0) + \frac{\mu}{2} \cdot \epsilon \right) + \mu \cdot \left\| \mathbf{W}_1(0) \mathbf{X} \right\|_{\max} \cdot \sigma_1(\mathbf{W}_2) \cdot \left(\beta \cdot \sigma_1(\mathbf{W}_2) \cdot \sqrt{d} \cdot \epsilon + \left\| \mathbf{Y} \right\|_F \right).$$

If $\mathbf{W}_1^\top(0) \mathbf{W}_1(0) = \epsilon^2 \mathbf{I}_d$, where ϵ satisfies $r(\epsilon) < \frac{\phi'(0) \cdot \sigma_K(\mathbf{W}_2^\top \mathbf{Y} \mathbf{X}^\top)}{2}$, then, for all $i \in [d]$, we have

$$\sigma_i(\mathbf{G}_1(0)) \in \begin{cases} [\phi'(0) \cdot \sigma_i(\mathbf{W}_2^\top \mathbf{Y} \mathbf{X}^\top) - r(\epsilon), \phi'(0) \cdot \sigma_i(\mathbf{W}_2^\top \mathbf{Y} \mathbf{X}^\top) + r(\epsilon)] & i = 1, \dots, K \\ [0, r(\epsilon)] & i = K + 1, \dots, d \end{cases}$$

Proof. Recall from (12) that

$$\mathbf{G}_1(0) = (\mathbf{W}_2^\top \Delta_2(0) \odot \phi'(\mathbf{W}_1(0) \mathbf{X})) \mathbf{X}^\top.$$

Now, define a term $\mathbf{P}(0) := (\mathbf{W}_2^\top \Delta_2(0) \odot \phi'(\mathbf{W}_1(0) \mathbf{X})) - \phi'(0) \cdot \mathbf{W}_2^\top \Delta_2(0)$, and $\mathbf{\Gamma}(0) := \Delta_2(0) \mathbf{X}^\top$. This means

$$\mathbf{G}_1(0) = \phi'(0) \cdot \mathbf{W}_2^\top \Delta_2(0) \mathbf{X}^\top + \mathbf{P}(0) \mathbf{X}^\top = \phi'(0) \cdot \mathbf{W}_2^\top \mathbf{\Gamma}(0) + \mathbf{P}(0) \mathbf{X}^\top. \quad (14)$$

Here, $\phi'(0) \cdot \mathbf{W}_2^\top \mathbf{\Gamma}(0)$ is the linear component of $\mathbf{G}_1(0)$, while $\mathbf{P}(0) \mathbf{X}^\top$ is a perturbation of $\phi'(0) \cdot \mathbf{W}_2^\top \mathbf{\Gamma}(0)$.

Singular values of $\mathbf{W}_2^\top \mathbf{\Gamma}(0)$. We first analyze the singular values of $\mathbf{W}_2^\top \mathbf{\Gamma}(0)$, which is (at most) rank- K . Note

$$\mathbf{W}_2^\top \mathbf{\Gamma}(0) = \mathbf{W}_2^\top \Delta_2(0) \mathbf{X}^\top = (\mathbf{W}_2^\top \mathbf{W}_2 \phi(\mathbf{W}_1(0) \mathbf{X}) - \mathbf{W}_2^\top \mathbf{Y}) \mathbf{X}^\top = (\mathbf{W}_2^\top \mathbf{W}_2 \phi(\mathbf{W}_1(0) \mathbf{X}) \mathbf{X}^\top - \mathbf{W}_2^\top \mathbf{Y} \mathbf{X}^\top).$$

Also note

$$\begin{aligned}
\sigma_1(\mathbf{W}_2^\top \mathbf{W}_2 \phi(\mathbf{W}_1(0) \mathbf{X}) \mathbf{X}^\top) &\leq \sigma_1(\mathbf{W}_2^\top \mathbf{W}_2 \phi(\mathbf{W}_1(0) \mathbf{X})) \leq \sigma_1^2(\mathbf{W}_2) \cdot \sigma_1(\phi(\mathbf{W}_1(0) \mathbf{X})) \\
&\leq \sigma_1^2(\mathbf{W}_2) \cdot \left(\phi'(0) \cdot \sigma_1(\mathbf{Z}_1(0)) + \sigma_1(\mathbf{R}(\mathbf{Z}_1(0))) \right),
\end{aligned}$$

where the last inequality is from taking the Taylor expansion of $\phi(\mathbf{W}_1(0) \mathbf{X})$ element-wise around $\mathbf{0}_m \mathbf{0}_N^\top$, with $\mathbf{R}(\mathbf{Z}_1(0))$ denoting the remainder, and then applying the triangle inequality. Since $\mathbf{W}_1(0)$ is an ϵ -scaled

semi-orthogonal matrix, and $\mathbf{X}\mathbf{X}^\top = \mathbf{I}_d$, we have $\sigma_1(\mathbf{Z}_1(0)) \leq \sigma_1(\mathbf{W}_1(0)) = \epsilon$. Next, since $\phi(\cdot)$ is μ -smooth, by Taylor's Remainder Theorem (Spivak, 2006), we have

$$|\mathbf{R}(\mathbf{Z}_1(0))_{ij}| \leq \frac{\mu}{2} \left|(\mathbf{Z}_1(0))_{ij}\right|^2 = \frac{\mu}{2} (\mathbf{Z}_1(0))_{ij}^2,$$

or equivalently,

$$|\mathbf{R}(\mathbf{Z}_1(0))| \leq \frac{\mu}{2} (\mathbf{Z}_1(0) \odot \mathbf{Z}_1(0)),$$

where $|\cdot|$ and \leq are element-wise. We then have

$$\begin{aligned} \sigma_1(\mathbf{R}(\mathbf{Z}_1(0))) &\stackrel{(i)}{\leq} \sigma_1(|\mathbf{R}(\mathbf{Z}_1(0))|) \stackrel{(ii)}{\leq} \frac{\mu}{2} \cdot \sigma_1(\mathbf{Z}_1(0) \odot \mathbf{Z}_1(0)) \\ &\leq \frac{\mu}{2} \cdot \sqrt{\|\mathbf{Z}_1(0) \odot \mathbf{Z}_1(0)\|_\infty \|\mathbf{Z}_1(0) \odot \mathbf{Z}_1(0)\|_1} \\ &\stackrel{(iii)}{\leq} \frac{\mu}{2} \cdot \sqrt{\epsilon^2 \cdot \epsilon^2} = \frac{\mu}{2} \cdot \epsilon^2, \end{aligned}$$

where (i) is from Lemma D.1, (ii) is from Horn and Johnson (2012, Theorem 8.1.18), and (iii) is from Lemma D.2. In summary,

$$\begin{aligned} \sigma_1(\mathbf{W}_2^\top \mathbf{W}_2 \phi(\mathbf{W}_1(0)\mathbf{X})) &\leq \sigma_1^2(\mathbf{W}_2) \cdot (\phi'(0) \cdot \sigma_1(\mathbf{Z}_1(0)) + \sigma_1(\mathbf{R}(\mathbf{Z}_1(0)))) \\ &\leq \sigma_1^2(\mathbf{W}_2) \cdot \left(\phi'(0) \cdot \epsilon + \frac{\mu}{2} \cdot \epsilon^2 \right) = \epsilon \cdot \sigma_1^2(\mathbf{W}_2) \cdot \left(\phi'(0) + \frac{\mu}{2} \cdot \epsilon \right). \end{aligned}$$

Thus, by Weyl's inequality (Weyl, 1949):

$$|\sigma_i(\mathbf{W}_2^\top \mathbf{\Gamma}(0)) - \sigma_i(\mathbf{W}_2^\top \mathbf{Y}\mathbf{X}^\top)| \leq \sigma_1(\mathbf{W}_2^\top \mathbf{W}_2 \phi(\mathbf{W}_1(0)\mathbf{X})) \leq \epsilon \cdot \sigma_1^2(\mathbf{W}_2) \cdot \left(\phi'(0) + \frac{\mu}{2} \cdot \epsilon \right). \quad (15)$$

Let $r_1(\epsilon) := \epsilon \cdot \phi'(0) \cdot \sigma_1^2(\mathbf{W}_2) \cdot \left(\phi'(0) + \frac{\mu}{2} \cdot \epsilon \right)$. By rearranging (15), for all $i = 1, \dots, K$, we have

$$\phi'(0) \cdot \sigma_i(\mathbf{W}_2^\top \mathbf{Y}\mathbf{X}^\top) - r_1(\epsilon) \leq \phi'(0) \cdot \sigma_i(\mathbf{W}_2^\top \mathbf{\Gamma}(0)) \leq \phi'(0) \cdot \sigma_i(\mathbf{W}_2^\top \mathbf{Y}\mathbf{X}^\top) + r_1(\epsilon) \quad (16)$$

For $i = K+1, \dots, d$, we have $\sigma_i(\phi'(0) \cdot \mathbf{W}_2^\top \mathbf{\Gamma}(0)) = 0$ since $\mathbf{W}_2^\top \mathbf{\Gamma}(0)$ is at most rank- K .

Singular values of $\mathbf{G}_1(0)$. We now analyze the singular values of $\mathbf{G}_1(0)$. Recall $\phi'(x)$ is μ -Lipschitz over \mathbb{R} , so $|\phi'(x) - \phi'(0)| \leq \mu \cdot |x|$ for all $x \in \mathbb{R}$. Therefore,

$$\begin{aligned} |\phi'(\mathbf{W}_1(0)\mathbf{X})_{ij} - \phi'(0)| &\leq \mu \left| (\mathbf{W}_1(0)\mathbf{X})_{ij} \right| \leq \mu \cdot \|\mathbf{W}_1(0)\mathbf{X}\|_{\max} \\ &\implies \phi'(0) - \mu \cdot \|\mathbf{W}_1(0)\mathbf{X}\|_{\max} \leq \phi'(\mathbf{W}_1(0)\mathbf{X})_{ij} \leq \phi'(0) + \mu \cdot \|\mathbf{W}_1(0)\mathbf{X}\|_{\max} \\ &\implies -\mu \cdot \|\mathbf{W}_1(0)\mathbf{X}\|_{\max} \leq \phi'(\mathbf{W}_1(0)\mathbf{X})_{ij} - \phi'(0) \leq \mu \cdot \|\mathbf{W}_1(0)\mathbf{X}\|_{\max}. \end{aligned}$$

Therefore,

$$-\mu \cdot \|\mathbf{W}_1(0)\mathbf{X}\|_{\max} \cdot (\mathbf{W}_2^\top \Delta_2(0))_{ij} \leq \underbrace{(\mathbf{W}_2^\top \Delta_2(0))_{ij} \cdot (\phi'(\mathbf{W}_1(0)\mathbf{X})_{ij} - \phi'(0))}_{:=(\mathbf{P}(0))_{ij}} \leq \mu \cdot \|\mathbf{W}_1(0)\mathbf{X}\|_{\max} \cdot (\mathbf{W}_2^\top \Delta_2(0))_{ij}.$$

As a result,

$$|(\mathbf{P}(0))_{ij}| \leq \mu \cdot \|\mathbf{W}_1(0)\mathbf{X}\|_{\max} \cdot |(\mathbf{W}_2^\top \Delta_2(0))_{ij}| \implies \|\mathbf{P}(0)\|_F \leq \mu \cdot \|\mathbf{W}_1(0)\mathbf{X}\|_{\max} \cdot \|\mathbf{W}_2^\top \Delta_2(0)\|_F.$$

Note $\|\mathbf{W}_2^\top \Delta_2(0)\|_F \leq \sigma_1(\mathbf{W}_2) \cdot \|\Delta_2(0)\|_F$, and so

$$\|\mathbf{W}_2^\top \Delta_2(0)\|_F \leq \sigma_1(\mathbf{W}_2) \cdot \|\mathbf{W}_2 \phi(\mathbf{W}_1(0)\mathbf{X}) - \mathbf{Y}\|_F \leq \sigma_1(\mathbf{W}_2) \cdot \left(\beta \cdot \sigma_1(\mathbf{W}_2) \cdot \sqrt{d} \cdot \epsilon + \|\mathbf{Y}\|_F \right)$$

Again by Weyl's inequality, Equation (14), and Equation (16),

$$\begin{aligned} |\sigma_i(\mathbf{G}_1(0)) - \phi'(0) \cdot \sigma_i(\mathbf{W}_2^\top \mathbf{\Gamma}(0))| &\leq \sigma_1(\mathbf{P}(0)\mathbf{X}^\top) \leq \|\mathbf{P}(0)\mathbf{X}^\top\|_F \\ &\leq \mu \cdot \|\mathbf{W}_1(0)\mathbf{X}\|_{\max} \cdot \|\mathbf{W}_2^\top \mathbf{\Delta}_2(0)\|_F \leq \mu \cdot \|\mathbf{W}_1(0)\mathbf{X}\|_{\max} \cdot \sigma_1(\mathbf{W}_2) \cdot \left(\beta \cdot \sigma_1(\mathbf{W}_2) \cdot \sqrt{d} \cdot \epsilon + \|\mathbf{Y}\|_F \right). \end{aligned}$$

Let $r_2(\epsilon) := \mu \cdot \|\mathbf{W}_1(0)\mathbf{X}\|_{\max} \cdot \sigma_1(\mathbf{W}_2) \cdot \left(\beta \cdot \sigma_1(\mathbf{W}_2) \cdot \sqrt{d} \cdot \epsilon + \|\mathbf{Y}\|_F \right)$. Therefore, for all $i \in [d]$, we have

$$\begin{aligned} \phi'(0) \cdot \sigma_i(\mathbf{W}_2^\top \mathbf{\Gamma}(0)) - r_2(\epsilon) &\leq \sigma_i(\mathbf{G}_1(0)) \leq \phi'(0) \cdot \sigma_i(\mathbf{W}_2^\top \mathbf{\Gamma}(0)) + r_2(\epsilon) \\ \implies \phi'(0) \cdot \sigma_i(\mathbf{W}_2^\top \mathbf{Y}\mathbf{X}^\top) - r_1(\epsilon) - r_2(\epsilon) &\leq \sigma_i(\mathbf{G}_1(0)) \leq \phi'(0) \cdot \sigma_i(\mathbf{W}_2^\top \mathbf{Y}\mathbf{X}^\top) + r_1(\epsilon) + r_2(\epsilon). \end{aligned}$$

Define $r(\epsilon) = r_1(\epsilon) + r_2(\epsilon)$. Since $\mathbf{W}_2^\top \mathbf{Y}\mathbf{X}^\top$ is rank- K , for all $i \in [d]$, we have

$$\sigma_i(\mathbf{G}_1(0)) \in \begin{cases} [\phi'(0) \cdot \sigma_i(\mathbf{W}_2^\top \mathbf{Y}\mathbf{X}^\top) - r(\epsilon), \phi'(0) \cdot \sigma_i(\mathbf{W}_2^\top \mathbf{Y}\mathbf{X}^\top) + r(\epsilon)] & i = 1, \dots, K \\ [0, r(\epsilon)] & i = K+1, \dots, d \end{cases}$$

Finally, note that we require $\sigma_K(\mathbf{G}_1(0)) - \sigma_{K+1}(\mathbf{G}_1(0)) > 0$, which implies

$$\phi'(0) \cdot \sigma_K(\mathbf{W}_2^\top \mathbf{Y}\mathbf{X}^\top) - 2 \cdot r(\epsilon) > 0 \implies r(\epsilon) < \frac{\phi'(0) \cdot \sigma_K(\mathbf{W}_2^\top \mathbf{Y}\mathbf{X}^\top)}{2},$$

which completes the proof. \square

Our next result characterizes how the bottom $d - K$ left and singular subspaces change between $\mathbf{G}_1(t)$ and $\mathbf{G}_1(0)$.

Lemma D.9. *Suppose Assumptions 3.2 through 3.4 hold. Define*

$$\gamma_L := \mu \cdot M \cdot \|\mathbf{W}_2\|_1 + \beta^2 \cdot \sigma_1^2(\mathbf{W}_2), \quad \text{and}$$

$$r(\epsilon) = \epsilon \cdot \phi'(0) \cdot \sigma_1^2(\mathbf{W}_2) \cdot \left(\phi'(0) + \frac{\mu}{2} \cdot \epsilon \right) + \mu \cdot \|\mathbf{W}_1(0)\mathbf{X}\|_{\max} \cdot \sigma_1(\mathbf{W}_2) \cdot \left(\beta \cdot \sigma_1(\mathbf{W}_2) \cdot \sqrt{d} \cdot \epsilon + \|\mathbf{Y}\|_F \right).$$

If $\mathbf{W}_1^\top(0)\mathbf{W}_1(0) = \epsilon^2 \mathbf{I}_d$ where ϵ satisfies $r(\epsilon) < \frac{\phi'(0) \cdot \sigma_K(\mathbf{W}_2^\top \mathbf{Y}\mathbf{X}^\top)}{2}$, and $\eta \leq \frac{1}{\gamma_L}$, then for all $t \geq 1$, we have

$$\begin{aligned} \left\| \mathbf{L}_{1,1}^\top(t) \mathbf{L}_{1,2}(0) \right\|_F &\leq \frac{\gamma_L \cdot \beta \cdot \sigma_1(\mathbf{W}_2) \cdot \sqrt{2\ell(0)} \cdot \Theta(1) \cdot \left(1 - (1 - \Theta(\eta))^{\Theta(t)} \right)}{\phi'(0) \cdot \sigma_K(\mathbf{W}_2^\top \mathbf{Y}\mathbf{X}^\top) - r(\epsilon) - \sigma_{K+1}(\mathbf{G}_1(t))}, \quad \text{and} \\ \left\| \mathbf{R}_{1,1}^\top(t) \mathbf{R}_{1,2}(0) \right\|_F &\leq \frac{\gamma_L \cdot \beta \cdot \sigma_1(\mathbf{W}_2) \cdot \sqrt{2\ell(0)} \cdot \Theta(1) \cdot \left(1 - (1 - \Theta(\eta))^{\Theta(t)} \right)}{\phi'(0) \cdot \sigma_K(\mathbf{W}_2^\top \mathbf{Y}\mathbf{X}^\top) - r(\epsilon) - \sigma_{K+1}(\mathbf{G}_1(t))}, \end{aligned}$$

which provides upper bounds on the change in the top- K left and right singular subspaces of $\mathbf{G}_1(t)$ from $\mathbf{G}_1(0)$.

Proof. Before proceeding, we note that at $t = 0$, we have $\text{dist}(\mathbf{W}_1^\top(0)\mathbf{L}_{1,1}(t)/\epsilon, \mathbf{W}_1^\top(0)\mathbf{L}_{1,1}(0)/\epsilon) = \text{dist}(\mathbf{R}_{1,2}(t), \mathbf{R}_{1,2}(0)) = 0$ exactly, so we consider $t \geq 1$. This is an direct application of Wedin's Sin Theorem (Lemma D.5). We first upper bound $\|\mathbf{G}_1(t) - \mathbf{G}_1(0)\|_F$:

$$\begin{aligned} \|\mathbf{G}_1(t) - \mathbf{G}_1(0)\|_F &\stackrel{(i)}{\leq} \gamma_L \cdot \|\mathbf{W}_1(t) - \mathbf{W}_1(0)\|_F = \gamma_L \cdot \eta \cdot \left\| \sum_{\tau=0}^{t-1} \mathbf{G}_1(\tau) \right\|_F \\ &\leq \gamma_L \cdot \eta \cdot \sum_{\tau=0}^{t-1} \|\mathbf{G}_1(\tau)\|_F \stackrel{(ii)}{\leq} \gamma_L \cdot \eta \cdot \|\mathbf{G}_1(0)\|_F \cdot \sum_{\tau=0}^{t-1} (1 - \Theta(\eta))^{\Theta(\tau)} \\ &\stackrel{(iii)}{\leq} \gamma_L \cdot \beta \cdot \eta \cdot \sigma_1(\mathbf{W}_2) \cdot \sqrt{2\ell(0)} \cdot \sum_{\tau=0}^{t-1} (1 - \Theta(\eta))^{\Theta(\tau)} \end{aligned}$$

$$\begin{aligned}
&\leq \gamma_L \cdot \beta \cdot \eta \cdot \sigma_1(\mathbf{W}_2) \cdot \sqrt{2\ell(0)} \cdot \frac{1 - (1 - \Theta(\eta))^{\Theta(t)}}{\Theta(\eta)} \\
&= \gamma_L \cdot \beta \cdot \sigma_1(\mathbf{W}_2) \cdot \sqrt{2\ell(0)} \cdot \Theta(1) \cdot \left(1 - (1 - \Theta(\eta))^{\Theta(t)}\right),
\end{aligned}$$

where (i) is from Lemma D.7, (ii) is from Assumption 3.4, and (iii) is from Lemma D.6. Then, directly from Wedin's Sin Theorem (Lemma D.5) Lemma D.3,

$$\|\mathbf{R}_{1,1}^\top(t)\mathbf{R}_{1,2}(0)\|_F \leq \frac{\|\mathbf{G}_1(t) - \mathbf{G}_1(0)\|_F}{\sigma_K(\mathbf{G}_1(0)) - \sigma_{K+1}(\mathbf{G}_1(t))} \leq \frac{\gamma_L \cdot \beta \cdot \sigma_1(\mathbf{W}_2) \cdot \sqrt{2\ell(0)} \cdot \Theta(1) \cdot \left(1 - (1 - \Theta(\eta))^{\Theta(t)}\right)}{\phi'(0) \cdot \sigma_K(\mathbf{W}_2^\top \mathbf{Y} \mathbf{X}^\top) - r(\epsilon) - \sigma_{K+1}(\mathbf{G}_1(t))}, \quad (17)$$

which also applies to $\|\mathbf{L}_{1,1}^\top(t)\mathbf{L}_{1,2}(0)\|_F$. Note from Assumption 3.4 and our condition on $r(\epsilon)$, the denominator is strictly positive. This completes the proof. \square

D.4 Proof of Theorem 3.5

In this section, we provide a proof of Theorem 3.5. First, we provide a result that identifies a p -dimensional subspace where $\mathbf{G}_1(t)$ has a bounded component for all $t \geq 0$ — Theorem 3.5 follows straightforwardly after.

Lemma D.10. *Suppose Assumptions 3.2 through 3.4 hold. Define*

$$\begin{aligned}
\gamma_L &= \mu \cdot M \cdot \|\mathbf{W}_2\|_1 + \beta^2 \cdot \sigma_1^2(\mathbf{W}_2), \\
r(\epsilon) &= \epsilon \cdot \phi'(0) \cdot \sigma_1^2(\mathbf{W}_2) \cdot \left(\phi'(0) + \frac{\mu}{2} \cdot \epsilon\right) + \mu \cdot \|\mathbf{W}_1(0)\mathbf{X}\|_{\max} \cdot \sigma_1(\mathbf{W}_2) \cdot \left(\beta \cdot \sigma_1(\mathbf{W}_2) \cdot \sqrt{d} \cdot \epsilon + \|\mathbf{Y}\|_F\right), \\
A(t) &:= \max \left\{ \|\sin \Theta(\mathbf{L}_{1,1}(t), \mathbf{L}_{1,1}(0))\|_2, \|\sin \Theta(\mathbf{R}_{1,1}(t), \mathbf{R}_{1,1}(0))\|_2 \right\}, \quad \text{and} \\
\delta(t) &:= \frac{\gamma_L \cdot \beta \cdot \sigma_1(\mathbf{W}_2) \cdot \sqrt{2\ell(0)} \cdot \Theta(1) \cdot \left(1 - (1 - \Theta(\eta))^{\Theta(t)}\right)}{\phi'(0) \cdot \sigma_K(\mathbf{W}_2^\top \mathbf{Y} \mathbf{X}^\top) - r(\epsilon) - \sigma_{K+1}(\mathbf{G}_1(t))}.
\end{aligned}$$

If $\mathbf{W}_1^\top(0)\mathbf{W}_1(0) = \epsilon^2 \mathbf{I}_d$ where ϵ satisfies $r(\epsilon) < \frac{\phi'(0) \cdot \sigma_K(\mathbf{W}_2^\top \mathbf{Y} \mathbf{X}^\top)}{2}$, and $\eta \leq \frac{1}{\gamma_L}$, then there exist semi-orthogonal matrices $\mathbf{V} \in \mathbb{R}^{d \times p}$ and $\mathbf{U} \in \mathbb{R}^{m \times p}$ such that

$$\begin{aligned}
\mathbf{W}_1(0)\mathbf{V} &= \epsilon \mathbf{U}, \quad \mathbf{W}_1^\top(0)\mathbf{U} = \epsilon \mathbf{V}, \quad \text{and} \\
\max \left\{ \frac{\|\mathbf{W}_1(t+1)\mathbf{V} - \mathbf{W}_1(t)\mathbf{V}\|_F}{\sqrt{p}}, \frac{\|\mathbf{W}_1^\top(t+1)\mathbf{U} - \mathbf{W}_1^\top(t)\mathbf{U}\|_F}{\sqrt{p}} \right\} &\leq \eta \cdot \rho(t),
\end{aligned}$$

where

$$\begin{aligned}
\rho(t) &= \sqrt{\sigma_1^2(\mathbf{G}_1(t)) \cdot \frac{A^2(t)}{p} + \sigma_{K+1}^2(\mathbf{G}_1(t))} \\
&\leq \begin{cases} \frac{r(\epsilon) \cdot \sqrt{p}}{\sqrt{\tilde{G}^2 \cdot (1 - \Theta(\eta))^{\Theta(t)} \cdot \frac{\delta^2(t)}{p} \cdot (\phi'(0) \cdot \sigma_1(\mathbf{W}_2^\top \mathbf{Y} \mathbf{X}^\top) + r(\epsilon))^2 + \sigma_{K+1}^2(\mathbf{G}_1(t))}}} & t = 0 \\ \frac{r(\epsilon) \cdot \sqrt{p}}{\sqrt{\tilde{G}^2 \cdot (1 - \Theta(\eta))^{\Theta(t)} \cdot \frac{\delta^2(t)}{p} \cdot (\phi'(0) \cdot \sigma_1(\mathbf{W}_2^\top \mathbf{Y} \mathbf{X}^\top) + r(\epsilon))^2 + \sigma_{K+1}^2(\mathbf{G}_1(t))}}} & t \geq 1 \end{cases}.
\end{aligned}$$

where $\tilde{G} := G_1 \cdot G_2$.

Proof. Define

$$\mathcal{S} := \mathcal{R}(\mathbf{R}_{1,2}(0)) \cap \mathcal{R}^\perp(\mathbf{W}_1^\top(0)\mathbf{L}_{1,1}(0)/\epsilon),$$

Both $\mathcal{R}(\mathbf{R}_{1,2}(0))$ and $\mathcal{R}^\perp(\mathbf{W}_1^\top(0)\mathbf{L}_{1,1}(0)/\epsilon)$ are of dimension $d - K$, so $\dim(\mathcal{S}) = d - 2K := p$. Let $\mathbf{V} \in \mathbb{R}^{d \times p}$ be an orthonormal basis for \mathcal{S} , and $\mathbf{U} := \mathbf{W}_1(0)\mathbf{V}/\epsilon \in \mathbb{R}^{m \times p}$. From the definitions of \mathbf{U} and \mathbf{V} , we trivially have

$$\mathbf{W}_1(0)\mathbf{V} - \epsilon\mathbf{U} = \mathbf{0}_{m \times p} \quad \text{and} \quad \mathbf{W}_1^\top(0)\mathbf{U} - \epsilon\mathbf{V} = \mathbf{0}_{d \times p}.$$

Now consider an arbitrary t for $t \geq 0$. From the GD update,

$$\begin{aligned} \|\mathbf{W}_1(t+1)\mathbf{V} - \mathbf{W}_1(t)\mathbf{V}\|_F &= \eta \cdot \|G_1(t)\mathbf{V}\|_F \quad \text{and} \\ \|\mathbf{W}_1^\top(t+1)\mathbf{U} - \mathbf{W}_1^\top(t)\mathbf{U}\|_F &= \eta \cdot \|G_1^\top(t)\mathbf{U}\|_F. \end{aligned}$$

We first upper bound $\|G_1(t)\mathbf{V}\|_F$, which then also applies for $\|G_1^\top(t)\mathbf{U}\|_F$.

Upper bounding $\|G_1(t)\mathbf{V}\|_F$ and $\|G_1^\top(t)\mathbf{U}\|_F$. Recall $G_1(t) = \mathbf{L}_{1,1}(t)\Sigma_{1,1}(t)\mathbf{R}_{1,1}^\top(t) + \mathbf{L}_{1,2}(t)\Sigma_{1,2}(t)\mathbf{R}_{1,2}^\top(t)$. Therefore,

$$\begin{aligned} G_1(t)\mathbf{V} &= \mathbf{L}_{1,1}(t)\Sigma_{1,1}(t)\mathbf{R}_{1,1}^\top(t)\mathbf{V} + \mathbf{L}_{1,2}(t)\Sigma_{1,2}(t)\mathbf{R}_{1,2}^\top(t)\mathbf{V} \\ \implies \|G_1(t)\mathbf{V}\|_F &= \sqrt{\left\|\mathbf{L}_{1,1}(t)\Sigma_{1,1}(t)\mathbf{R}_{1,1}^\top(t)\mathbf{V}\right\|_F^2 + \left\|\mathbf{L}_{1,2}(t)\Sigma_{1,2}(t)\mathbf{R}_{1,2}^\top(t)\mathbf{V}\right\|_F^2} \\ &= \sqrt{\left\|\Sigma_{1,1}(t)\mathbf{R}_{1,1}^\top(t)\mathbf{V}\right\|_F^2 + \left\|\Sigma_{1,2}(t)\mathbf{R}_{1,2}^\top(t)\mathbf{V}\right\|_F^2} \\ &\leq \sqrt{\sigma_1^2(G_1(t)) \cdot \left\|\mathbf{R}_{1,1}^\top(t)\mathbf{V}\right\|_F^2 + \sigma_{K+1}^2(G_1(t)) \cdot \left\|\mathbf{R}_{1,2}^\top(t)\mathbf{V}\right\|_F^2} \\ &\leq \sqrt{\sigma_1^2(G_1(t)) \cdot \left\|\mathbf{R}_{1,1}^\top(t)\mathbf{R}_{1,1}(0)\right\|_F^2 + \sigma_{K+1}^2(G_1(t)) \cdot \left\|\mathbf{R}_{1,2}^\top(t)\mathbf{V}\right\|_F^2} \\ &\stackrel{(i)}{=} \sqrt{\underbrace{\sigma_1^2(G_1(t)) \cdot \|\sin \Theta(\mathbf{R}_{1,1}(t), \mathbf{R}_{1,1}(0))\|_2^2}_{(a)} + \underbrace{\sigma_{K+1}^2(G_1(t)) \cdot \left\|\mathbf{R}_{1,2}^\top(t)\mathbf{V}\right\|_F^2}_{(b)}}. \end{aligned}$$

where (i) is from Lemma D.3. Next, define $\mathbf{W}_1(0) := \epsilon\mathbf{Q} \implies \mathbf{Q} := \mathbf{W}_1(0)/\epsilon$ and $\tilde{\mathbf{L}}_{1,2}(0)$ to be an orthonormal basis for $\mathcal{R}^\perp(\mathbf{W}_1^\top(0)\mathbf{L}_{1,1}(0)/\epsilon) = \mathcal{R}^\perp(\mathbf{Q}^\top\mathbf{L}_{1,1}(0))$. Recall by definition, we have $\mathbf{V} \in \mathcal{R}(\tilde{\mathbf{L}}_{1,2}(0))$. Therefore,

$$\begin{aligned} G_1^\top(t)\mathbf{U} &= \mathbf{R}_{1,1}(t)\Sigma_{1,1}^\top(t)\mathbf{L}_{1,1}^\top(t)\mathbf{U} + \mathbf{R}_{1,2}(t)\Sigma_{1,2}^\top(t)\mathbf{L}_{1,2}^\top(t)\mathbf{U} \\ \implies \|G_1^\top(t)\mathbf{U}\|_F &= \sqrt{\|\mathbf{R}_{1,1}(t)\Sigma_{1,1}^\top(t)\mathbf{L}_{1,1}^\top(t)\mathbf{U}\|_F^2 + \|\mathbf{R}_{1,2}(t)\Sigma_{1,2}^\top(t)\mathbf{L}_{1,2}^\top(t)\mathbf{U}\|_F^2} \\ &= \sqrt{\|\Sigma_{1,1}^\top(t)\mathbf{L}_{1,1}^\top(t)\mathbf{U}\|_F^2 + \|\Sigma_{1,2}^\top(t)\mathbf{L}_{1,2}^\top(t)\mathbf{U}\|_F^2} \\ &\leq \sqrt{\sigma_1^2(G_1(t)) \cdot \|\mathbf{L}_{1,1}^\top(t)\mathbf{U}\|_F^2 + \sigma_{K+1}^2(G_1(t)) \cdot \|\mathbf{L}_{1,2}^\top(t)\mathbf{U}\|_F^2} \\ &= \sqrt{\sigma_1^2(G_1(t)) \cdot \|\mathbf{L}_{1,1}^\top(t)\mathbf{W}_1(0)\mathbf{V}/\epsilon\|_F^2 + \sigma_{K+1}^2(G_1(t)) \cdot \|\mathbf{L}_{1,2}^\top(t)\mathbf{W}_1(0)\mathbf{V}/\epsilon\|_F^2} \\ &:= \sqrt{\sigma_1^2(G_1(t)) \cdot \|\mathbf{L}_{1,1}^\top(t)\mathbf{Q}\mathbf{V}\|_F^2 + \sigma_{K+1}^2(G_1(t)) \cdot \|\mathbf{L}_{1,2}^\top(t)\mathbf{Q}\mathbf{V}\|_F^2} \\ &\leq \sqrt{\sigma_1^2(G_1(t)) \cdot \|\mathbf{L}_{1,1}^\top(t)\mathbf{Q}\tilde{\mathbf{L}}_{1,2}(0)\|_F^2 + \sigma_{K+1}^2(G_1(t)) \cdot \|\mathbf{L}_{1,2}^\top(t)\mathbf{Q}\mathbf{V}\|_F^2} \\ &\stackrel{(ii)}{\leq} \sqrt{\sigma_1^2(G_1(t)) \cdot \|\mathbf{L}_{1,1}^\top(t)\mathbf{L}_{1,2}(0)\|_F^2 + \sigma_{K+1}^2(G_1(t)) \cdot \|\mathbf{L}_{1,2}^\top(t)\mathbf{Q}\mathbf{V}\|_F^2} \\ &\stackrel{(iii)}{=} \sqrt{\underbrace{\sigma_1^2(G_1(t)) \cdot \|\sin \Theta(\mathbf{L}_{1,1}(t), \mathbf{L}_{1,1}(0))\|_F^2}_{(c)} + \underbrace{\sigma_{K+1}^2(G_1(t)) \cdot \|\mathbf{L}_{1,2}^\top(t)\mathbf{Q}\mathbf{V}\|_F^2}_{(d)}}. \end{aligned}$$

where (ii) is from Lemma D.4, and (iii) is from Lemma D.3. The definition of $A(t)$, combined with the fact that $\|\mathbf{R}_{1,2}^\top(t)\mathbf{V}\|_F^2 \leq p$ and $\|\mathbf{L}_{1,2}^\top(t)\mathbf{Q}\mathbf{V}\|_F^2 \leq p$, gives us

$$\max \left\{ \|\mathbf{G}_1(t)\mathbf{V}\|_F, \|\mathbf{G}_1^\top(t)\mathbf{U}\|_F \right\} \leq \sqrt{\sigma_1^2(\mathbf{G}_1(t)) \cdot A^2(t) + \sigma_{K+1}^2(\mathbf{G}_1(t)) \cdot p} := \rho(t) \cdot \sqrt{p}.$$

To upper bound $\rho(t) \cdot \sqrt{p}$, we upper bound (a) and (c). We have already provided upper bounds for (b) and (d) via through $\|\mathbf{R}_{1,2}^\top(t)\mathbf{V}\|_F^2 \leq p$ and $\|\mathbf{L}_{1,2}^\top(t)\mathbf{Q}\mathbf{V}\|_F^2 \leq p$.

Upper bounding (a) and (c). First, note that at $t = 0$, we have (a) = 0, and (b) = $\sigma_{K+1}^2(\mathbf{G}_1(0)) \cdot p = r^2(\epsilon) \cdot p$. Thus, we focus on $t \geq 1$. We first focus on (a). Recall by definition, $\mathbf{V} \in \mathcal{R}(\mathbf{R}_{1,2}(0))$. From Lemma D.9, we have

$$\|\sin \Theta(\mathbf{R}_{1,1}(t), \mathbf{R}_{1,1}(0))\|_2 \leq \delta(t) \implies (a) \leq \sigma_1^2(\mathbf{G}_1(t)) \cdot \|\sin \Theta(\mathbf{R}_{1,1}(t), \mathbf{R}_{1,1}(0))\|_2^2 \leq \sigma_1^2(\mathbf{G}_1(t)) \cdot \delta^2(t).$$

Then, from Assumption 3.4, we have

$$\frac{\sigma_1(\mathbf{G}_1(t))}{\sigma_1(\mathbf{G}_1(0))} \leq G_2 \cdot \frac{\|\mathbf{G}_1(t)\|_F}{\|\mathbf{G}_1(0)\|_F} \leq G_2 \cdot G_1 \cdot (1 - \Theta(\eta))^{\Theta(t)} \implies \sigma_1(\mathbf{G}_1(t)) \leq \bar{G} \cdot (1 - \Theta(\eta))^{\Theta(t)} \cdot \sigma_1(\mathbf{G}_1(0)).$$

where $\bar{G} := G_2 \cdot G_1$. From Lemma D.8, we have

$$\begin{aligned} (a) &\leq \bar{G}^2 \cdot (1 - \Theta(\eta))^{\Theta(t)} \cdot \delta^2(t) \cdot \sigma_1^2(\mathbf{G}_1(0)) \\ &\leq \bar{G}^2 \cdot (1 - \Theta(\eta))^{\Theta(t)} \cdot \delta^2(t) \cdot (\phi'(0) \cdot \sigma_1(\mathbf{W}_2^\top \mathbf{Y} \mathbf{X}^\top) + r(\epsilon))^2. \end{aligned}$$

To upper bound (c), note from Lemma D.9, we have $\|\sin \Theta(\mathbf{L}_{1,1}(t), \mathbf{L}_{1,1}(0))\|_2 \leq \delta(t)$. Thus, the steps to upper bound (c) are equivalent to the steps to upper bound (a). In summary,

$$\rho(t) \cdot \sqrt{p} \leq \begin{cases} \frac{r(\epsilon) \cdot \sqrt{p}}{t = 0} \\ \sqrt{\bar{G}^2 \cdot (1 - \Theta(\eta))^{\Theta(t)} \cdot \delta^2(t) \cdot (\phi'(0) \cdot \sigma_1(\mathbf{W}_2^\top \mathbf{Y} \mathbf{X}^\top) + r(\epsilon))^2 + \sigma_{K+1}^2(\mathbf{G}_1(t)) \cdot p} \quad t \geq 1 \end{cases}.$$

Final result. Combining everything together yields

$$\begin{aligned} \|\mathbf{W}_1(t+1)\mathbf{V} - \mathbf{W}_1(t)\mathbf{V}\|_F &\leq \eta \cdot \rho(t) \cdot \sqrt{p} \quad \text{and} \\ \|\mathbf{W}_1^\top(t+1)\mathbf{U} - \mathbf{W}_1^\top(t)\mathbf{U}\|_F &\leq \eta \cdot \rho(t) \cdot \sqrt{p}, \end{aligned}$$

where

$$\begin{aligned} \rho(t) &:= \sqrt{\sigma_1^2(\mathbf{G}_1(t)) \cdot \frac{A^2(t)}{p} + \sigma_{K+1}^2(\mathbf{G}_1(t))} \\ &\leq \begin{cases} \frac{r(\epsilon) \cdot \sqrt{p}}{t = 0} \\ \sqrt{\bar{G}^2 \cdot (1 - \Theta(\eta))^{\Theta(t)} \cdot \frac{\delta^2(t)}{p} \cdot (\phi'(0) \cdot \sigma_1(\mathbf{W}_2^\top \mathbf{Y} \mathbf{X}^\top) + r(\epsilon))^2 + \sigma_{K+1}^2(\mathbf{G}_1(t))} \quad t \geq 1 \end{cases}. \end{aligned}$$

Dividing both sides by \sqrt{p} completes the proof. \square

We now provide a proof of Theorem 3.5. We re-state the (formal) Theorem statement here for convenience.

Theorem D.11 (Formal version of Theorem 3.5). *Suppose Assumptions 3.2 through 3.4 hold. Define*

$$\begin{aligned} \gamma_L &:= \mu \cdot M \cdot \|\mathbf{W}_2\|_1 + \beta^2 \cdot \sigma_1^2(\mathbf{W}_2), \\ r(\epsilon) &:= \epsilon \cdot \phi'(0) \cdot \sigma_1^2(\mathbf{W}_2) \cdot \left(\phi'(0) + \frac{\mu}{2} \epsilon \right) + \mu \cdot \|\mathbf{W}_1(0)\mathbf{X}\|_{\max} \cdot \sigma_1(\mathbf{W}_2) \cdot \left(\beta \cdot \sigma_1(\mathbf{W}_2) \cdot \sqrt{d} \cdot \epsilon + \|\mathbf{Y}\|_F \right), \\ A(t) &:= \max \left\{ \|\sin \Theta(\mathbf{L}_{1,1}(t), \mathbf{L}_{1,1}(0))\|_2, \|\sin \Theta(\mathbf{R}_{1,1}(t), \mathbf{R}_{1,1}(0))\|_2 \right\}, \quad \text{and} \end{aligned}$$

$$\delta(t) := \frac{\gamma_L \cdot \beta \cdot \sigma_1(\mathbf{W}_2) \cdot \sqrt{2\ell(0)} \cdot \Theta(1) \cdot \left(1 - (1 - \Theta(\eta))^{\Theta(t)}\right)}{\phi'(0) \cdot \sigma_K(\mathbf{W}_2^\top \mathbf{Y} \mathbf{X}^\top) - r(\epsilon) - \sigma_{K+1}(\mathbf{G}_1(t))}.$$

If $\mathbf{W}_1^\top(0)\mathbf{W}_1(0) = \epsilon^2 \mathbf{I}_d$ where ϵ satisfies $r(\epsilon) < \frac{\phi'(0) \cdot \sigma_K(\mathbf{W}_2^\top \mathbf{Y} \mathbf{X}^\top)}{2}$, and $\eta \leq \frac{1}{\gamma_L}$, then there exist orthogonal matrices $\mathbf{U} \in \mathbb{R}^{m \times m}$ and $\mathbf{V} \in \mathbb{R}^{d \times d}$ such that, for all $t \geq 0$, $\mathbf{W}_1(t)$ admits the following decomposition:

$$\mathbf{W}_1(t) = \mathbf{U} \widetilde{\mathbf{W}}_1(t) \mathbf{V}^\top = \mathbf{U} \begin{bmatrix} \widetilde{\mathbf{W}}_{1,1}(t) & \widetilde{\mathbf{W}}_{1,2}(t) \\ \widetilde{\mathbf{W}}_{1,3}(t) & \widetilde{\mathbf{W}}_{1,4}(t) \end{bmatrix} \mathbf{V}^\top,$$

where $\widetilde{\mathbf{W}}_{1,1} \in \mathbb{R}^{(m-p) \times 2K}$, $\widetilde{\mathbf{W}}_{1,2} \in \mathbb{R}^{(m-p) \times p}$, $\widetilde{\mathbf{W}}_{1,3} \in \mathbb{R}^{p \times 2K}$, and $\widetilde{\mathbf{W}}_{1,4} \in \mathbb{R}^{p \times p}$, with

$$\widetilde{\mathbf{W}}_{1,2}(0) = \mathbf{0}_{(m-p) \times p}, \quad \widetilde{\mathbf{W}}_{1,3}(0) = \mathbf{0}_{p \times 2K}, \quad \frac{\|\widetilde{\mathbf{W}}_{1,4}(0)\|_F}{\sqrt{p}} = \epsilon,$$

and

$$\frac{\|\widetilde{\mathbf{W}}_{1,i}(t+1) - \widetilde{\mathbf{W}}_{1,i}(t)\|_F}{\sqrt{p}} \leq \eta \cdot \rho(t)$$

for all $i \in \{2, 3, 4\}$, where

$$\begin{aligned} \rho(t) &= \sqrt{\sigma_1^2(\mathbf{G}_1(t)) \cdot \frac{A^2(t)}{p} + \sigma_{K+1}^2(\mathbf{G}_1(t))} \\ &\leq \begin{cases} r(\epsilon) \cdot \sqrt{p} & t = 0 \\ \sqrt{\bar{G}^2 \cdot (1 - \Theta(\eta))^{\Theta(t)} \cdot \frac{\delta^2(t)}{p} \cdot (\phi'(0) \cdot \sigma_1(\mathbf{W}_2^\top \mathbf{Y} \mathbf{X}^\top) + r(\epsilon))^2 + \sigma_{K+1}^2(\mathbf{G}_1(t))} & t \geq 1 \end{cases}. \end{aligned}$$

Proof. From Lemma D.10, there exist $\mathbf{V}_2 \in \mathbb{R}^{d \times p}$ and $\mathbf{U}_2 \in \mathbb{R}^{m \times p}$ with orthonormal columns such that for any $t \geq 0$:

$$\mathbf{W}_1(t+1)\mathbf{V}_2 = \mathbf{W}_1(t)\mathbf{V}_2 + \mathbf{T}_1(t),$$

where $\|\mathbf{T}_1(t)\|_F \leq \eta \cdot \rho(t)$, and $\mathbf{W}_1(0)\mathbf{V}_2 = \epsilon \mathbf{U}_2$. Similarly,

$$\mathbf{W}_1^\top(t+1)\mathbf{U}_2 = \mathbf{W}_1^\top(t)\mathbf{U}_2 + \mathbf{T}_2(t),$$

where again $\|\mathbf{T}_2(t)\|_F \leq \eta \cdot \rho(t)$ and $\mathbf{W}_1^\top(0)\mathbf{U} = \epsilon \mathbf{V}$. Complete \mathbf{V}_2 and \mathbf{U}_2 to be orthogonal matrices, defined as $\mathbf{V} := [\mathbf{V}_1 \ \mathbf{V}_2] \in \mathbb{R}^{d \times d}$ and $\mathbf{U} := [\mathbf{U}_1 \ \mathbf{U}_2] \in \mathbb{R}^{m \times m}$. Then, we have

$$\begin{aligned} \mathbf{U}_1^\top \mathbf{W}_1(t+1)\mathbf{V}_2 - \mathbf{U}_1^\top \mathbf{W}_1(t)\mathbf{V}_2 &= \mathbf{U}_1^\top \mathbf{T}_1(t) \\ \implies \|\mathbf{U}_1^\top \mathbf{W}_1(t+1)\mathbf{V}_2 - \mathbf{U}_1^\top \mathbf{W}_1(t)\mathbf{V}_2\|_F &= \|\mathbf{U}_1^\top \mathbf{T}_1(t)\|_F \leq \|\mathbf{T}_1(t)\|_F \leq \eta \cdot \rho(t), \end{aligned}$$

where

$$\mathbf{U}_1^\top \mathbf{W}_1(0)\mathbf{V}_2 = \epsilon \mathbf{U}_1^\top \mathbf{U}_2 = \mathbf{0}_{2K \times p} \implies \|\mathbf{U}_1^\top \mathbf{W}_1(0)\mathbf{V}_2\|_F = 0.$$

Similarly, we have

$$\|\mathbf{V}_1^\top \mathbf{W}_1(t+1)\mathbf{U}_2 - \mathbf{V}_1^\top \mathbf{W}_1(t)\mathbf{U}_2\|_F = \|\mathbf{V}_1^\top \mathbf{T}_2(t)\|_F \leq \|\mathbf{T}_2(t)\|_F \leq \eta \cdot \rho(t),$$

where

$$\mathbf{V}_1^\top \mathbf{W}_1^\top(0)\mathbf{U}_2 = \epsilon \mathbf{V}_1^\top \mathbf{V}_2 = \mathbf{0}_{2K \times p} \implies \|\mathbf{V}_1^\top \mathbf{W}_1(0)\mathbf{U}_2\|_F = 0.$$

Finally, we have

$$\|\mathbf{U}_2^\top \mathbf{W}_1(t+1) \mathbf{V}_2 - \mathbf{U}_2^\top \mathbf{W}_1(t) \mathbf{V}_2\|_F = \|\mathbf{U}_2^\top \mathbf{T}_1(t)\|_F \leq \eta \cdot \rho(t),$$

where

$$\mathbf{U}_2^\top \mathbf{W}_1(0) \mathbf{V}_2 = \epsilon \mathbf{U}_2^\top \mathbf{U}_2 = \epsilon \mathbf{I}_p \implies \|\mathbf{U}_2^\top \mathbf{W}_1(0) \mathbf{V}_2\|_F = \epsilon \sqrt{p}.$$

Putting everything together:

$$\mathbf{U}^\top \mathbf{W}_1(t) \mathbf{V} = \begin{bmatrix} \mathbf{U}_1^\top \\ \mathbf{U}_2^\top \end{bmatrix} \mathbf{W}_1(t) \begin{bmatrix} \mathbf{V}_1 & \mathbf{V}_2 \end{bmatrix} = \begin{bmatrix} \mathbf{U}_1^\top \mathbf{W}_1(t) \mathbf{V}_1 & \mathbf{U}_1^\top \mathbf{W}_1(t) \mathbf{V}_2 \\ \mathbf{U}_2^\top \mathbf{W}_1(t) \mathbf{V}_1 & \mathbf{U}_2^\top \mathbf{W}_1(t) \mathbf{V}_2 \end{bmatrix} := \begin{bmatrix} \widetilde{\mathbf{W}}_{1,1}(t) & \widetilde{\mathbf{W}}_{1,2}(t) \\ \widetilde{\mathbf{W}}_{1,3}(t) & \widetilde{\mathbf{W}}_{1,4}(t) \end{bmatrix},$$

where

$$\begin{aligned} \|\widetilde{\mathbf{W}}_{1,2}(0)\|_F &= \|\mathbf{U}_1^\top \mathbf{W}_1(0) \mathbf{V}_2\|_F = 0 \\ \|\widetilde{\mathbf{W}}_{1,3}(0)\|_F &= \|\mathbf{U}_2^\top \mathbf{W}_1(0) \mathbf{V}_1\|_F = 0, \quad \text{and} \\ \|\widetilde{\mathbf{W}}_{1,4}(0)\|_F &= \|\mathbf{U}_2^\top \mathbf{W}_1(0) \mathbf{V}_2\|_F = \epsilon \sqrt{p}, \end{aligned}$$

as well as

$$\begin{aligned} \|\widetilde{\mathbf{W}}_{1,2}(t+1) - \widetilde{\mathbf{W}}_{1,2}(t)\|_F &= \|\mathbf{U}_1^\top \mathbf{W}_1(t+1) \mathbf{V}_2 - \mathbf{U}_1^\top \mathbf{W}_1(t) \mathbf{V}_2\|_F \leq \eta \cdot \rho(t), \\ \|\widetilde{\mathbf{W}}_{1,3}(t+1) - \widetilde{\mathbf{W}}_{1,3}(t)\|_F &= \|\mathbf{U}_2^\top \mathbf{W}_1(t+1) \mathbf{V}_1 - \mathbf{U}_2^\top \mathbf{W}_1(t) \mathbf{V}_1\|_F \leq \eta \cdot \rho(t), \quad \text{and} \\ \|\widetilde{\mathbf{W}}_{1,4}(t+1) - \widetilde{\mathbf{W}}_{1,4}(t)\|_F &= \|\mathbf{U}_2^\top \mathbf{W}_1(t+1) \mathbf{V}_2 - \mathbf{U}_2^\top \mathbf{W}_1(t) \mathbf{V}_2\|_F \leq \eta \cdot \rho(t). \end{aligned}$$

This completes the proof. \square

E Proof of Proposition B.1

In this section, we provide a proof of Proposition B.1. We use the same notation as in Appendix D. We re-state Proposition B.1 below for convenience.

Proposition E.1 (Proposition B.1 re-stated). *Suppose $d = N$, $\mathbf{W}_1(0)_{ij} \stackrel{iid}{\sim} \mathcal{N}\left(0, \frac{\epsilon^2}{m}\right)$, and $\phi = \text{ReLU}$. With probability at least $1 - \delta$ w.r.t. the randomness in $\mathbf{W}_1(0)$,*

$$\sigma_{d-K}(\mathbf{G}_1(0)) \geq \sqrt{\frac{\lambda_{\min}(\mathbf{V}^\top \mathbf{D} \mathbf{V})}{4} - \left(\frac{R'}{6} \cdot \log\left(\frac{2(d-K)}{\delta}\right) + \sqrt{2 \cdot \log\left(\frac{2(d-K)}{\delta}\right) \cdot \frac{R' \cdot \lambda_{\max}(\mathbf{V}^\top \mathbf{D} \mathbf{V})}{16}} \right)},$$

where \mathbf{V} is an orthonormal basis for $\mathcal{N}(\mathbf{W}_2^\top \Delta_2(0))$, $\mathbf{D} := \text{diag}\left(\left\|(\mathbf{W}_2^\top \Delta_2(0))_{:,1}\right\|_2^2, \dots, \left\|(\mathbf{W}_2^\top \Delta_2(0))_{:,N}\right\|_2^2\right)$, and $R' := \max_{i \in [m]} \left\|(\mathbf{W}_2^\top \Delta_2(0))_{i,:}\right\|_2^2$.

Proof. Recall that

$$\mathbf{G}_1(0) = (\mathbf{W}_2^\top \Delta_2(0) \odot \phi'(\mathbf{W}_1(0) \mathbf{X})) \mathbf{X}^\top.$$

Since $d = N$ and $\mathbf{X} \mathbf{X}^\top = \mathbf{I}_d$, \mathbf{X} is exactly an orthogonal matrix. Therefore, we have

$$\sigma_{d-K}(\mathbf{G}_1(0)) = \sigma_{d-K}(\mathbf{W}_2^\top \Delta_2(0) \odot \phi'(\mathbf{W}_1(0) \mathbf{X})),$$

so we aim to lower bound $\sigma_{K+1}(\mathbf{W}_2^\top \Delta_2(0) \odot \phi'(\mathbf{W}_1(0) \mathbf{X}))$. First, note that $\mathbf{W}_2^\top \Delta_2(0)$ is rank- K . Next, define $\mathbf{M} := \phi'(\mathbf{W}_1(0) \mathbf{X})$. Notice that \mathbf{M} contains iid Bernoulli entries with probability parameter $q = 0.5$, as

$(W_1(0)X)_{ij} \stackrel{iid}{\sim} \mathcal{N}\left(0, \frac{\epsilon^2}{m}\right)$, and $\phi'(W_1(0)X)_{ij} = \mathbb{I}\left[(W_1(0)X)_{ij} > 0\right]$, where \mathbb{I} denotes the indicator function. Finally, note $\mathbf{M} = q\mathbf{1}_m\mathbf{1}_N^\top + (\mathbf{M} - q\mathbf{1}_m\mathbf{1}_N^\top)$. Combining everything yields

$$W_2^\top \Delta_2(0) \odot \mathbf{M} = \underbrace{qW_2^\top \Delta_2(0)}_{:=S} + \underbrace{W_2^\top \Delta_2(0) \odot (\mathbf{M} - q\mathbf{1}_m\mathbf{1}_N^\top)}_{:=N}.$$

Therefore,

$$\begin{aligned} \sigma_{d-K}(W_2^\top \Delta_2(0) \odot \phi'(W_1(0)X)) &= \sigma_{d-K}(S + N) \\ &\stackrel{(i)}{=} \max_{\mathcal{T} \subset \mathbb{R}^N : \dim(\mathcal{T}) = d-K} \min_{x \in \mathcal{T}, \|x\|_2=1} \|(S + N)x\|_2 \\ &\stackrel{(ii)}{\geq} \min_{x \in \mathcal{N}(S), \|x\|_2=1} \|(S + N)x\|_2 = \min_{x \in \mathcal{N}(S), \|x\|_2=1} \|Nx\|_2. \end{aligned}$$

where (i) is from the Courant-Fischer Min-Max Theorem for singular values, i.e., [Horn and Johnson \(2012, Theorem 4.2.2\)](#) applied to $(S + N)^\top (S + N)$, and (ii) is using the fact that $\dim(\mathcal{N}(S)) = d - K$. Let $\mathbf{V} \in \mathbb{R}^{N \times (d-K)}$ be an orthonormal basis for $\mathcal{N}(S)$. Then,

$$\min_{x \in \mathcal{N}(S), \|x\|_2=1} \|Nx\|_2 = \min_{z \in \mathbb{R}^{d-K}, \|z\|_2=1} \|NVz\|_2 = \sigma_{\min}(NV).$$

Now, it suffices to lower bound $\sigma_{\min}(NV)$. Notice $NV \in \mathbb{R}^{m \times (d-K)}$ with $m \geq N > d - K$. Therefore, $\sigma_{\min}^2(NV) = \lambda_{\min}(\mathbf{V}^\top NV^\top NV)$, so we aim to lower bound $\lambda_{\min}(\mathbf{V}^\top NV^\top NV)$. Let $\widetilde{\mathbf{M}} := \mathbf{M} - q\mathbf{1}_m\mathbf{1}_N^\top$ and $\mathbf{E} = W_2^\top \Delta_2(0)$, so $N = \mathbf{E} \odot \widetilde{\mathbf{M}}$. Then,

$$\mathbf{V}^\top NV^\top NV = \mathbb{E}_N [\mathbf{V}^\top NV^\top NV] + (\mathbf{V}^\top NV^\top NV - \mathbb{E}_N [\mathbf{V}^\top NV^\top NV]),$$

and so by Weyl's inequality ([Weyl, 1949](#)),

$$\begin{aligned} \lambda_{\min}(\mathbf{V}^\top NV^\top NV) &= \lambda_{\min}(\mathbb{E}_N [\mathbf{V}^\top NV^\top NV] + (\mathbf{V}^\top NV^\top NV - \mathbb{E}_N [\mathbf{V}^\top NV^\top NV])) \\ &\geq \lambda_{\min}(\mathbb{E}_N [\mathbf{V}^\top NV^\top NV]) + \lambda_{\min}(\mathbf{V}^\top NV^\top NV - \mathbb{E}_N [\mathbf{V}^\top NV^\top NV]) \\ &\geq \underbrace{\lambda_{\min}(\mathbb{E}_N [\mathbf{V}^\top NV^\top NV])}_{(a)} - \underbrace{\sigma_1(\mathbf{V}^\top NV^\top NV - \mathbb{E}_N [\mathbf{V}^\top NV^\top NV])}_{(b)} \end{aligned}$$

We analyze (a) and (b) individually. To do so, we first determine $\mathbb{E}_N [\mathbf{V}^\top NV^\top NV]$.

Expectation of $\mathbf{V}^\top NV^\top NV$. First, since \mathbf{V} is deterministic w.r.t. N , we have

$$\mathbb{E}_N [\mathbf{V}^\top NV^\top NV] = \mathbf{V}^\top \mathbb{E}_{\widetilde{\mathbf{M}}} \left[(\mathbf{E} \odot \widetilde{\mathbf{M}})^\top (\mathbf{E} \odot \widetilde{\mathbf{M}}) \right] \mathbf{V}.$$

Therefore,

$$\begin{aligned} \left((\mathbf{E} \odot \widetilde{\mathbf{M}})^\top (\mathbf{E} \odot \widetilde{\mathbf{M}}) \right)_{ij} &= (\mathbf{E} \odot \widetilde{\mathbf{M}})^\top_{:,i} (\mathbf{E} \odot \widetilde{\mathbf{M}})_{:,j} = \sum_{k=1}^m (\mathbf{E} \odot \widetilde{\mathbf{M}})_{ki} (\mathbf{E} \odot \widetilde{\mathbf{M}})_{kj} = \sum_{k=1}^m \mathbf{E}_{ki} \mathbf{E}_{kj} \cdot \widetilde{\mathbf{M}}_{ki} \widetilde{\mathbf{M}}_{kj} \\ &\implies \mathbb{E}_{\widetilde{\mathbf{M}}} \left[\left((\mathbf{E} \odot \widetilde{\mathbf{M}})^\top (\mathbf{E} \odot \widetilde{\mathbf{M}}) \right)_{ij} \right] = \sum_{k=1}^m \mathbf{E}_{ki} \mathbf{E}_{kj} \cdot \mathbb{E} [\widetilde{\mathbf{M}}_{ki} \widetilde{\mathbf{M}}_{kj}] = \begin{cases} 0 & i \neq j \\ q^2 \cdot \|\mathbf{E}_{:,i}\|_2^2 & i = j \end{cases} \\ &\implies \mathbb{E}_{\widetilde{\mathbf{M}}} \left[(\mathbf{E} \odot \widetilde{\mathbf{M}})^\top (\mathbf{E} \odot \widetilde{\mathbf{M}}) \right] = q^2 \cdot \text{diag}(\|\mathbf{E}_{:,1}\|_2^2, \dots, \|\mathbf{E}_{:,N}\|_2^2) := q^2 \cdot \mathbf{D} \\ &\implies \mathbb{E}_N [\mathbf{V}^\top NV^\top NV] = q^2 \cdot \mathbf{V}^\top \mathbf{D} \mathbf{V}, \end{aligned}$$

where $\mathbf{A}_{:,i}$ denotes the i^{th} column in the matrix \mathbf{A} . Thus, we have

$$(a) = \lambda_{\min}(\mathbb{E}_N [\mathbf{V}^\top NV^\top NV]) = q^2 \cdot \lambda_{\min}(\mathbf{V}^\top \mathbf{D} \mathbf{V}),$$

so now we aim to lower bound (b).

Bounding (b). We aim to use the Matrix Bernstein inequality, i.e., [Tropp et al. \(2015, Theorem 6.1.1\)](#) to bound (b). First, define $\bar{N} := V^\top N^\top NV - \mathbb{E}_N [V^\top N^\top NV]$. Note we can write \bar{N} as a sum of independent, zero-mean, symmetric random matrices:

$$V^\top N^\top NV - \mathbb{E}_N [V^\top N^\top NV] = \sum_{i=1}^m V^\top (E \odot \bar{M})_{i,:} (E \odot \bar{M})_{i,:}^\top V - \mathbb{E} \left[V^\top (E \odot \bar{M})_{i,:} (E \odot \bar{M})_{i,:}^\top V \right]$$

where $A_{i,:}$ denotes the i^{th} row in A , but written as a column vector. The terms in the sum are independent since the rows of \bar{M} are independent. Next, define $\mathbf{n}_i := V^\top (E \odot \bar{M})_{i,:}$ and $\bar{N}_i = \mathbf{n}_i \mathbf{n}_i^\top - \mathbb{E} [\mathbf{n}_i \mathbf{n}_i^\top]$. Then, we have $\bar{N} = \sum_{i=1}^m (\mathbf{n}_i \mathbf{n}_i^\top - \mathbb{E} [\mathbf{n}_i \mathbf{n}_i^\top]) = \sum_{i=1}^m \bar{N}_i$. To leverage the Matrix Bernstein inequality, we must bound $\sigma_1(\bar{N}_i)$ and $\nu(\bar{N}) := \sigma_1(\mathbb{E} [\bar{N}^2])$.

Bounding $\sigma_1(\bar{N}_i)$. We first bound $\sigma_1(\bar{N}_i)$. First, recall $\bar{N}_i = \mathbf{n}_i \mathbf{n}_i^\top - \mathbb{E} [\mathbf{n}_i \mathbf{n}_i^\top]$, and notice it is the difference of two symmetric matrices, and thus is itself symmetric. Therefore,

$$\sigma_1(\bar{N}_i) = \max \{ \lambda_{\max}(\mathbf{n}_i \mathbf{n}_i^\top - \mathbb{E} [\mathbf{n}_i \mathbf{n}_i^\top]), |\lambda_{\min}(\mathbf{n}_i \mathbf{n}_i^\top - \mathbb{E} [\mathbf{n}_i \mathbf{n}_i^\top])| \}.$$

Next, $\mathbf{n}_i \mathbf{n}_i^\top \succeq 0$ with probability 1, which implies $\mathbb{E} [\mathbf{n}_i \mathbf{n}_i^\top] \succeq 0$. Therefore,

$$\lambda_{\max}(\mathbf{n}_i \mathbf{n}_i^\top - \mathbb{E} [\mathbf{n}_i \mathbf{n}_i^\top]) \leq \lambda_{\max}(\mathbf{n}_i \mathbf{n}_i^\top) = \|\mathbf{n}_i\|_2^2,$$

and

$$\begin{aligned} \lambda_{\min}(\mathbf{n}_i \mathbf{n}_i^\top - \mathbb{E} [\mathbf{n}_i \mathbf{n}_i^\top]) &\geq \lambda_{\min}(-\mathbb{E} [\mathbf{n}_i \mathbf{n}_i^\top]) = -\lambda_{\max}(\mathbb{E} [\mathbf{n}_i \mathbf{n}_i^\top]) \\ \implies |\lambda_{\min}(\mathbf{n}_i \mathbf{n}_i^\top - \mathbb{E} [\mathbf{n}_i \mathbf{n}_i^\top])| &\leq \lambda_{\max}(\mathbb{E} [\mathbf{n}_i \mathbf{n}_i^\top]) \stackrel{(i)}{\leq} \mathbb{E} [\lambda_{\max}(\mathbf{n}_i \mathbf{n}_i^\top)] = \mathbb{E} [\|\mathbf{n}_i\|_2^2], \end{aligned}$$

where (i) is from Jensen's inequality. Thus, we focus on analyzing $\|\mathbf{n}_i\|_2^2$. Note

$$\mathbf{n}_i = V^\top (E \odot \bar{M})_{i,:} = V^\top \text{diag}(E_{i,:}) \bar{M}_{i,:},$$

where $\text{diag}(\mathbf{a})$ is a diagonal matrix whose entries are the elements of the vector \mathbf{a} . Therefore,

$$\begin{aligned} \|\mathbf{n}_i\|_2^2 &= \mathbf{n}_i^\top \mathbf{n}_i = \bar{M}_{i,:}^\top \text{diag}(E_{i,:})^\top V V^\top \text{diag}(E_{i,:}) \bar{M}_{i,:} \stackrel{(ii)}{\leq} \bar{M}_{i,:}^\top \text{diag}(E_{i,:})^\top \text{diag}(E_{i,:}) \bar{M}_{i,:} = q^2 \|E_{i,:}\|_2^2 \\ \implies \|\mathbf{n}_i\|_2^2 &\leq q^2 \cdot \max_{i \in [m]} \|E_{i,:}\|_2^2 := q^2 \cdot R' \end{aligned}$$

with probability 1, where (ii) is because $V V^\top \leq I_N$. Therefore, for all $i \in [m]$,

$$\sigma_1(\bar{N}_i) = \max \{ \lambda_{\max}(\mathbf{n}_i \mathbf{n}_i^\top - \mathbb{E} [\mathbf{n}_i \mathbf{n}_i^\top]), |\lambda_{\min}(\mathbf{n}_i \mathbf{n}_i^\top - \mathbb{E} [\mathbf{n}_i \mathbf{n}_i^\top])| \} \leq \max \{ \|\mathbf{n}_i\|_2^2, \mathbb{E} [\|\mathbf{n}_i\|_2^2] \} \leq q^2 \cdot R'$$

with probability 1.

Bounding $\nu(\bar{N})$. Next, we bound $\nu(\bar{N}) = \sigma_1(\mathbb{E} [\bar{N}^2])$. Since each \bar{N}_i is zero mean, we have

$$\sigma_1(\mathbb{E} [\bar{N}^2]) = \sigma_1 \left(\sum_{i=1}^m \mathbb{E} [\bar{N}_i^2] \right).$$

For an arbitrary $i \in [m]$:

$$\begin{aligned}\mathbb{E} [\bar{N}_i^2] &= \mathbb{E} [(n_i n_i^\top - \mathbb{E} [n_i n_i])^2] = \mathbb{E} [(n_i n_i^\top)^2] - \mathbb{E} [n_i n_i^\top]^2 \\ &= \mathbb{E} [\|n_i\|_2^2 \cdot n_i n_i^\top] - \mathbb{E} [n_i n_i^\top]^2 \stackrel{(ii)}{\leq} q^2 \cdot R' \cdot \mathbb{E} [n_i n_i^\top] - \mathbb{E} [n_i n_i^\top]^2 \leq q^2 \cdot R' \cdot \mathbb{E} [n_i n_i^\top]\end{aligned}$$

where (ii) is from the fact that $\|n_i\|_2^2 \leq q^2 \cdot R'$ with probability 1. Therefore,

$$\sum_{i=1}^m \mathbb{E} [\bar{N}_i^2] \leq q^2 \cdot R' \cdot \sum_{i=1}^m \mathbb{E} [n_i n_i^\top] \stackrel{(iii)}{=} q^2 \cdot R' \cdot \mathbb{E}_N [V^\top N^\top N V] = q^4 \cdot R' \cdot V^\top D V,$$

where (iii) is because $n_i := V^\top (E \odot \bar{M})_{i,:} = V^\top N_{i,:}$, and so $\sum_{i=1}^m n_i n_i^\top = V^\top N^\top N V$. As a result,

$$\sigma_1 (\mathbb{E} [\bar{N}^2]) = \sigma_1 \left(\sum_{i=1}^m \mathbb{E} [\bar{N}_i^2] \right) \leq q^4 \cdot R' \cdot \lambda_{\max} (V^\top D V)$$

Matrix Bernstein inequality. From [Tropp et al. \(2015\)](#), Theorem 6.1.1), for all $\tau \geq 0$:

$$\begin{aligned}\mathbb{P} (\sigma_1 (\bar{N}) \geq \tau) &\leq 2(d - K) \cdot \exp \left(\frac{-\tau^2/2}{\nu (\bar{N}) + \max_i \sigma_1 (\bar{N}_i) \cdot \tau/3} \right) \\ &\leq 2(d - K) \cdot \exp \left(\frac{-\tau^2/2}{q^4 \cdot R' \cdot \lambda_{\max} (V^\top D V) + q^2 \cdot R' \cdot \tau/3} \right) \leq \delta,\end{aligned}$$

which implies

$$\tau \geq \frac{q^2 \cdot R'}{3} \cdot \log \left(\frac{2(d - K)}{\delta} \right) + \sqrt{\left(\frac{q^2 \cdot R'}{3} \cdot \log \left(\frac{2(d - K)}{\delta} \right) \right)^2 + 2 \cdot \log \left(\frac{2(d - K)}{\delta} \right) \cdot (q^4 \cdot R' \cdot \lambda_{\max} (V^\top D V))}.$$

Using $\sqrt{a + b} \leq \sqrt{a} + \sqrt{b}$, a sufficient condition is

$$\tau \geq \frac{2q^2 \cdot R'}{3} \cdot \log \left(\frac{2(d - K)}{\delta} \right) + \sqrt{2 \cdot \log \left(\frac{2(d - K)}{\delta} \right) \cdot (q^4 \cdot R' \cdot \lambda_{\max} (V^\top D V))}.$$

Therefore, with probability at least $1 - \delta$,

$$\sigma_1 (\bar{N}) \leq \frac{2q^2 \cdot R'}{3} \cdot \log \left(\frac{2(d - K)}{\delta} \right) + \sqrt{2 \cdot \log \left(\frac{2(d - K)}{\delta} \right) \cdot (q^4 \cdot R' \cdot \lambda_{\max} (V^\top D V))}.$$

Final result. Putting everything together, for any $\delta \in (0, 1)$, with probability at least $1 - \delta$,

$$\sigma_{d-K} (G_1(0)) \geq \sqrt{q^2 \cdot \lambda_{\min} (V^\top D V) - \left(\frac{2q^2 \cdot R'}{3} \cdot \log \left(\frac{2(d - K)}{\delta} \right) + \sqrt{2 \cdot \log \left(\frac{2(d - K)}{\delta} \right) \cdot (q^4 \cdot R' \cdot \lambda_{\max} (V^\top D V))} \right)}.$$

Substituting $q = 0.5$ completes the proof. □

F Low-Rank MLP Ablations

In this section, we provide ablation studies on the initialization of the \tilde{U} and \tilde{V} factors, as well as the width parameter r . We ran all experiments in this section using PyTorch on an NVIDIA A100 GPU.

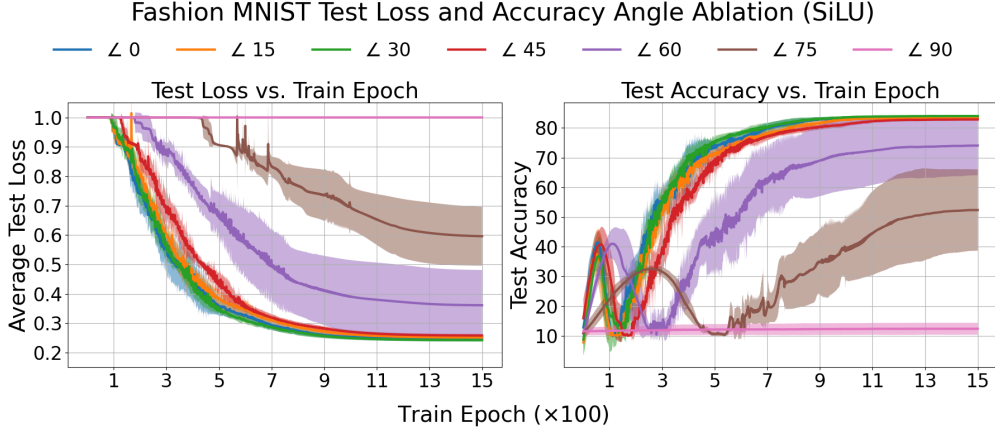


Figure 14: For all low-rank MLPs with \tilde{U} and \tilde{V} initialized close to ($\psi \leq 45$ degrees) \tilde{U}_{big} and \tilde{V}_{big} , GD reaches similar solutions. Otherwise, GD gets stuck in progressively worse local minima as ψ increases.

F.1 Subspace Initialization

From Figures 6 and 7 in Sections 5.1.1 and 5.1.2 respectively, we observe that if we train the low-rank MLP in (10) after initializing \tilde{U} and \tilde{V} as random semi-orthogonal matrices (green), then (S)GD gets stuck in a much worse local minimum compared to the other MLPs (blue and orange). In this section, we ablate the initialization of \tilde{U} and \tilde{V} .

Experimental details. We repeated the experiments as described in Section 5.1.1. We used the exact same training algorithm (full batch GD), hyperparameters, and loss function (total squared-error loss). However, we only used $\phi = \text{SiLU}$, and we varied the initialization of \tilde{U} and \tilde{V} as follows. First, we define $\tilde{U}_{big} \in \mathbb{R}^{d \times r}$ and $\tilde{V}_{big} \in \mathbb{R}^{d \times r}$ to be the result of the \mathcal{S}_{big} initialization scheme described in Section 5, where we set $r = 2K = 20$. Next, we define $\tilde{U}_{big}^\perp, \tilde{V}_{big}^\perp \in \mathbb{R}^{d \times r}$ to be completely orthogonal to \tilde{U}_{big} and \tilde{V}_{big} , respectively. Finally, we initialized \tilde{U} and \tilde{V} to be some angle ψ degrees away from \tilde{U}_{big} and \tilde{V}_{big} via

$$\tilde{U} = \cos(\psi) \cdot \tilde{U}_{big} + \sin(\psi) \cdot \tilde{U}_{big}^\perp \quad \text{and} \quad \tilde{V} = \cos(\psi) \cdot \tilde{V}_{big} + \sin(\psi) \cdot \tilde{V}_{big}^\perp. \quad (18)$$

In our experiments, we swept through $\psi \in \{0, 15, 30, 45, 60, 75, 90\}$ degrees.

Results. Figure 14 shows the resulting test loss and accuracy curves during training averaged over 5 trials for each ψ . The test loss and accuracy curves are nearly identical for all $\psi \in \{0, 15, 30, 45\}$ degrees, although at $\psi = 45$, GD required slightly more iterations for the test loss to begin decreasing from its initial value. The performance noticeably deteriorates when $\psi > 45$. For $\psi \in \{60, 75\}$ degrees, the test loss still decreases from their initial values, but GD gets stuck in noticeably worse local minima compared to when $\psi < 45$. Finally, at $\psi = 90$, the initialized \tilde{U} and \tilde{V} are completely orthogonal to \tilde{U}_{big} and \tilde{V}_{big} . The test loss stays at its initial value for all training epochs, and the low-rank MLP does not escape the random guessing stage. Overall, if \tilde{U} / \tilde{V} in the low-rank MLP are initialized to be closer to $\tilde{U}_{big} / \tilde{V}_{big}$ than their orthogonal complements, then the low-rank MLP can eventually nearly match the performance of the full-rank counterpart. Otherwise, GD gets stuck in progressively worse local minima as $\psi \rightarrow 90$ degrees.

F.2 Width Ablation

From the classifier-only results in Section 5.1.2 (Figure 7), there is a 5 – 10% gap in test accuracy between the low-rank MLP with \mathcal{S}_{big} initialization (orange) and the fully parameterized MLP (blue). In this section, we investigate how much does this gap close by increasing the width r .

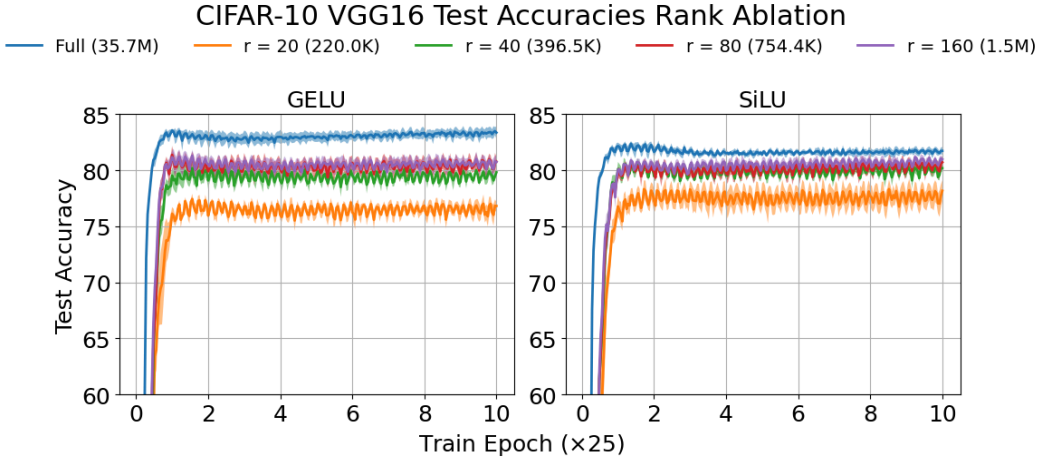


Figure 15: Increasing the width r of the low-rank MLP initially leads to a noticeable increase in test accuracy, but further increasing r leads to diminishing returns in test accuracy gains. Here, we only trained the classifier head in VGG-16, and kept the convolutional layers frozen at their ImageNet pre-trained weights.

Experimental details. We repeated the classifier-only training experiments as described in Section 5.1.2 with both $\phi = \text{GELU}$ and $\phi = \text{SiLU}$, again using the exact same training algorithm (SGD with momentum), hyper-parameters, and loss function (cross-entropy loss). However, now we vary the width $r \in \{2K, 4K, 8K, 16K\}$ in the low-rank MLP in (10). We initialized $\tilde{\mathbf{U}}$ and $\tilde{\mathbf{V}}$ using the \mathcal{S}_{big} initialization scheme as described in Section 5. For $r > 2K$, we initialized the last $r - 2K$ columns of $\tilde{\mathbf{U}}$ and $\tilde{\mathbf{V}}$ to lie in the orthogonal complements of their first $2K$ columns.

Results. Figure 15 shows the test accuracy at every training epoch for each r . Even going from $r = 2K$ to $r = 4K$ noticeably closes the gap between the low-rank and fully-parameterized MLPs, especially for the SiLU classifier. However, continuing to double r further leads to diminishing returns in performance gains. Nevertheless, with the appropriate initialization on $\tilde{\mathbf{U}}$ and $\tilde{\mathbf{V}}$, a width of $r = \Theta(K)$ appears to be sufficient in achieving a test accuracy that is only about 2 – 3% lower than that of the fully parameterized classifier head.